Title
The Structural Analysis of OMpC

Author
Chang, C.-F.

Publication Date
2017-12-06

Lawrence Berkeley Laboratory
UNIVERSITY OF CALIFORNIA

THE STRUCTURE ANALYSIS OF OmpC, ONE OF THE MAJOR PROTEINS IN THE OUTER MEMBRANE OF *E. coli*, BY HIGH RESOLUTION ELECTRON MICROSCOPY

C.-F. Chang
(Ph.D. Thesis)

July 1983

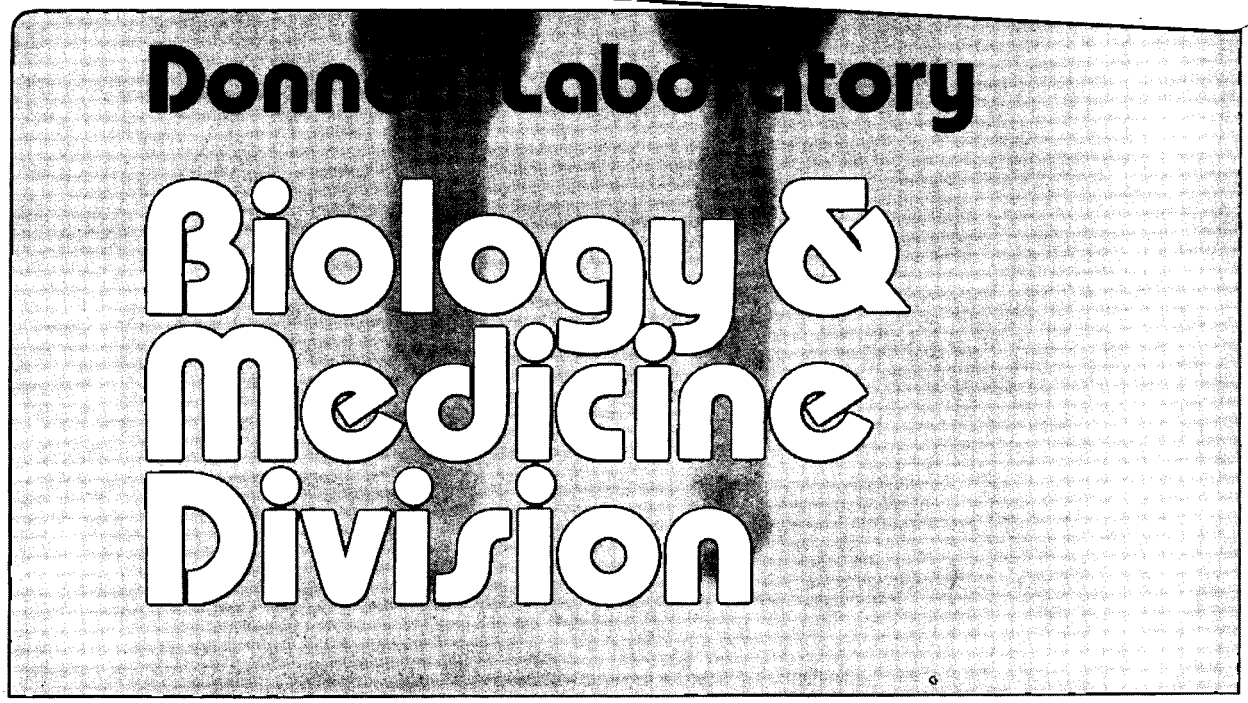

Prepared for the U.S. Department of Energy under Contract DE-AC03-76SF00098

DISCLAIMER

LBL-16341

THE STRUCTURE ANALYSIS OF OmpC, ONE OF THE MAJOR PROTEINS IN THE OUTER MEMBRANE OF *E. coli*, BY HIGH RESOLUTION ELECTRON MICROSCOPY

Chung-Fu Chang
(Ph.D. Thesis)

Lawrence Berkeley Laboratory
University of California
Berkeley, California 94720

July 1983

This work was supported by the U.S. Department of Energy under Contract Number DE-AC03-76SF0098.

TABLE OF CONTENTS

Acknowledgements

I would like to express my sincere appreciation to Professor Robert M. Glaeser for introducing me to the field of low dose, low temperature electron microscopy and for his continued support and general advice during the course of my graduate studies. I want to express my special thanks to Professor Shoji Mizushima for providing OmpC specimens; Professors Hiroshi Nikaido and Alexander V. Nichols for their careful reading and invaluable suggestions, and Dr. Margaret Newman for her help in correcting my English such that the thesis writing could be finished within a reasonable period.

I also want to thank members of our group, past and present, who deserve special thanks. Among them are Dr. David Grano, who developed the computer software so that the image processing was readily done; Dr. Kenneth Downing, whose dedication to the maintenance of the delicate microscope minimized the obstacles of data collection; Dr. Bing Jap, whose insights were always so helpful and supportive; Dr. Gina Sosinsky, who contributed tips on how to write the thesis through the NROFF program in the Unix system.

Finally, I deeply appreciate the encouragement from my wife, Tan, who patiently waited for me to finish this course of work.

ABSTRACT

The Structure Analysis of OmpC, One of the Major Proteins in the Outer Membrane of E. coli, by High Resolution Electron Microscopy

by

Chung-Fu Chang

This dissertation is concerned with the structure analysis of a pore-forming membrane protein, OmpC, which is one of the major proteins in the outer membrane of Escherichia coli. In order to obtain structural information it was necessary to develop a suitable technique for preparing two-dimensional crystalline arrays of this membrane protein in an unfixed, unstained and hydrated condition. Electron micrographs were recorded at exposures of less than 5 electrons/A^2 in order to avoid severe radiation damage. The resulting images were crystallographically averaged, in order to overcome the statistical limitations associated with the low electron exposures. The resulting images, which extend to a resolution of ~ 13.5 A, lend themselves to a natural interpretation that is consistent with the mass density of protein, water and lipid; prior data from 2-D and 3-D structure studies of

negatively stained specimens at ≈ 20 A resolution; and published spectroscopic data on the peptide chain secondary structure.

A technique, referred to here as the behenic acid monolayer technique, has been developed for preparing frozen-hydrated specimens suitable for low temperature electron microscopy. Bacteriorhodopsin from Halobacterium halobium was used as a test specimen for the technique. Electron diffraction patterns and low dose images of bR have been recorded and the structural information obtained from these studies extends to a resolution of at least ~ 7 A and 10 A respectively.

Low dose images of frozen-hydrated OmpC specimens yield optical diffraction patterns which show strong intensities at the (2,1) Bragg reflection, corresponding to a resolution ~ 25.4 A. Computer processing of such frozen-hydrated images retrieved structural information at a higher resolution. In order to assess the validity of the coefficients used in the image restoration, statistical evaluations of the signal-to-noise ratio of the coefficients have been carried out. Reliable data were obtained in this way out to a resolution of ~ 13.5 A.

Images of negatively stained OmpC specimens are also presented in this thesis. Comparing the computer processed images of negatively stained OmpC and frozen-

hydrated OmpC, we can identify a domain of the OmpC monomer which protrudes beyond the membrane bilayer, into the aqueous environment. From a single projection, however, it is not possible to determine on which side of the membrane this protruding mass is located. A simple and quick method which may obtain this extra information is proposed, by looking at the specimen which is freeze-dried and shadowed.

The expected density of lipid A, ~ 0.9 g/ml, is much lower than that of protein, 1.3 g/ml. It is therefore anticipated that the lipid regions should be quite distinct from the protein regions in the restored image. The water density, 1.0 g/ml, is also lower than that of protein. However, from the result of the 3-D structural studies, the water channels merge together as they span the membrane, and this structural feature causes a partial overlapping of aqueous domains and the protein domain, in the direction of the projection obtained in our images. The regions of the channels are therefore expected to be close to the averaged density of protein and water. Based on this information, we are able to identify the regions of protein, lipid A and channels.

The protein domain in the image of frozen-hydrated OmpC shows up as a narrow, elongated domain. From spectroscopic studies, it has been shown that OmpC has a high

content of β-structure. We therefore assign the protein domain as a projection of a layer of β-sheet, which spans the lipid bilayer perpendicularly.

CHAPTER 1

Introduction

In the last few years, research on the outer membrane proteins of Gram-negative bacteria has become extremely active. One reason is that the outer membrane contains a small variety of proteins in large quantities. These proteins are easily isolated and characterized. In addition, studies on the structure, function and biogenesis of these proteins have broad implications in many different areas of membrane biochemistry and molecular biology. Furthermore, one of the proteins in the mitochondrial outer membrane of rat liver and mung bean cells bears structural and functional similarities to OmpC and OmpF proteins in the outer membrane of Gram-negative bacteria (Zalman et al.,1980). Studies of these proteins in the procaryotic system may enable us to track the path of evolution through the eucaryotic system.

Researchers who study the outer membrane proteins are anxious to obtain structural information about these proteins in order to understand fully their function. In contrast to the knowledge we have about the biochemistry, physiology and genetics of the outer membrane proteins, the structural information we have about them is rather little. Therefore, structural investigations of the outer membrane proteins are needed.

Preliminary X-ray diffraction studies on OmpF, a major protein in the outer membrane of E. coli., have been reported (Garavito and Rosenbusch, 1980). The multiple isomorphous replacement (MIR) method must be used to retrieve the phase information of the structure factors of the protein. The MIR method requires at least two heavy atom derivatives of the protein in crystalline forms. Therefore, the three-dimensional, high-resolution structural information of OmpF is not readily forthcoming.

Using techniques of high resolution electron microscopy, the author has studied the structure of OmpC protein, which is functionally and structurally similar to OmpF. Reasons for performing the structural study by high resolution electron microscopy are: (a) The theory of image formation in an electron microscope allows us to directly retrieve the phase information of the structure factors. (b) The OmpC specimens that the author has studied were prepared by reconstituting purified OmpC trimers with lipid A (the core structure of the outer membrane lipopolysaccharide), while the 3-dimensional OmpF crystals made for the X-ray diffraction studies are grown in the presence of a detergent, n-octyl-α-glucopyranoside. In other words, the system that the author studies may be closer to the natural state of the protein. (The organization of the outer membrane will be mentioned later.)

(c) The OmpC specimens form well-ordered, two-dimensional periodic arrays which are excellent specimens for structural analysis by low dose, low temperature electron microscopy. Results presented in this thesis deal with the structural information contained in a single projection of frozen-hydrated OmpC specimens. Among other things, this information can serve as a reference available in the structural study of OmpF by X-ray crystallography. Furthermore, the frozen-hydrated specimen preparation techniques which will be discussed in Chapter 3, can be applied to the specimen preparation of many biological specimens.

1.1. Organization of the cell envelope of E. coli

The cell envelope of E. coli, a Gram-negative bacterium, contains three components: the outer membrane, the cell wall, which is a layer of peptidoglycan (PDG), and the cytoplasmic membrane. The outer membrane serves as a molecular sieve, providing a barrier and mediating communication with the environment. Several outer membrane proteins, referred to as porins,serve as pores to allow small hydrophilic molecules to diffuse across the membrane. The PDG layer, which binds covalently to the lipoprotein in the outer membrane, provides the mechanical and osmotic stability of the cell. The PDG layer is, however, a porous network. The cytoplasmic membrane actively

transports nutrients, which have diffused through the outer membrane, into the cell for the need of biosynthesis.

The space between the outer membrane and cytoplasmic membrane is referred to as the periplasmic space. Gram-negative bacteria use the periplasmic space to store some hydrolytic and cell-wall synthesizing enzymes and some binding proteins which are specific to certain amino acids and sugars. These binding proteins are further involved in transporting amino acids and sugars across the cytoplasmic membrane.

1.2. Components of the Outer Membrane

The outer membrane consists of a lipid bilayer in which both phospholipids and lipopolysaccharides are incorporated. However, lipopolysaccharides are incorporated only in the outer leaflet. This lipopolysaccharide monolayer is held together tightly through a combination of the hydrophobic interaction between the lipid tails and electro-static interactions between divalent cations and the carboxyl and phosphate groups on the lipopolysaccharide.

Proteins in the outer membrane are commonly defined as major and minor proteins, in terms of the numbers of molecules existing in the outer membrane. However, the

definition is rather arbitrary. A minor protein may become a major protein when its production is fully induced by specific growth conditions. Generally speaking, there are four major proteins in the wild-type strain of E. coli K-12, and there are ~ 20 minor proteins. Most of these minor proteins have been identified as receptors of bacteriophages and colicins.

The outer membrane proteins have been extensively reviewed by DiRienzo et al. (DiRienzo et al., 1978). Here we present a brief discussion of the major proteins in the outer membrane of E. coli. We name these proteins according to the nomenclature which is now commonly used.

1.2.1. OmpA

OmpA, which was designated as protein II*, 3a, B*, G, and d by different research groups, has molecular weight ~ 30,000. OmpA is required in the outer membrane of the F^- cells to allow stablization of mating contacts with F plasmid-carrying donor cells (Manning and Achtman, 1979). It had been postulated that OmpA forms a pore to transport molecules across the outer membrane (Manning et al., 1977). However, in a study of Salmonella typhimurium, another Gram-negative bacteria, it has been shown that the mutant strain of S. typhimurium lacking OmpA has no change in the rate of the transport of cephaloridine across the outer membrane (Nikaido et al., 1977).

1.2.2. Lipoprotein

Lipoprotein (M.W. ~ 7000) is the most abundant protein in the E. coli outer membrane, in terms of the number of the molecules (7.2×10^5 molecules/cell) (Inouye, 1979). The lipoprotein, also referred to as Braun lipoprotein, was first found covalently linked to the PDG (Braun and Rehn, 1969). However, free lipoprotein was later found in the the outer membrane as well (Inouye et al., 1972). Two thirds of the lipoprotein in the outer membrane is in the free state and the rest is bound to the PDG. The function of the lipoprotein is not fully understood yet. It has been shown, however, that the protein plays an important role in maintaining the outer membrane integrity (DiRienzo et al.,1978; Inouye, 1979).

1.2.3. OmpF

OmpF (M.W. ~ 36,500) was first purified and characterized by Rosenbusch (1974). OmpF contains 336 amino acid residues and it has a moderate hydrophobicity. Circular dichroism and infrared spectroscopy studies have shown this protein has a high content of β structure and no apparent α helix. In a study of the amino acid sequence of OmpF, Chen et al. (1979) found that the protein has no stretches of nonpolar residues longer than 11 amino acids. The nucleotide sequence of the structural gene that codes for OmpF has been reported by Inokuchi et

al. (1982).

Rosenbusch (1974) referred to OmpF as a "matrix" protein because the protein is tightly associated with the PDG layer and is arranged in two-dimensional periodic arrays. This protein was also designated as protein Ia, b, la, O-9 by other research groups.

OmpF forms an aqueous transmembrane channel allowing small hydrophilic solutes to diffuse across the outer membrane (Nakae, 1976). While the diffusion process has no chemical specificity regarding the solute, the process is size-selective. The largest solute molecule which can diffuse through the OmpF channel is of M.W. ~ 660 (Nakae and Nikaido, 1975).

Electron microscopy of negatively stained OmpF and of freeze-dried, shadowed OmpF indicates that the periodicity of OmpF arrays is still maintained in the absence of PDG (Steven et al., 1977). It was found in this study that trimeric OmpF molecules (with a three-fold rotational axis among three monomers) are arranged on a hexagonal lattice with a periodicity of 77Å. The most pronounced feature in the filtered images of negatively stained OmpF specimens is a triplet of stained region in each unit cell. The diameter of the stained regions is ~20Å, and the center-to-center distance between them is ~30Å. This feature represents the projected view of the OmpF channels, which

span the outer membrane.

Electrical conductance studies of OmpF molecules which have been incorporated into artificial, planar membranes indicated that: (1) The OmpF channels exist in open and closed states, and these two states are in equilibrium with each other. However, the application of a membrane potential shifts the equilibrium to the closed state. (2) The minimal open or closed unit consists of three channels with diameters of ~ 10Å at their narrowest region. (3) The channels open and close in a cooperative or concerted fashion; however, opening or closing can be clearly seen to occur in three discrete steps (Schindler and Rosenbusch, 1978).

An initial X-ray structural analysis of OmpF molecules which have been purified and recrystallized in the presence of n-octyl-α-glucopyranoside, was reported by Garavito and Rosenbusch (1980). In this study, the highest reflection order in the diffraction pattern corresponds to a resolution of 3.8Å. More recently, X-ray diffraction patterns of a tetragonal crystalline form of OmpF were recorded, using a synchrotron radiation source and an oscillation camera (Garavito et al., 1982). The diffraction spots extend out to ~ 2.9Å.

1.2.4. OmpC

OmpC (M.W. ~36,500), which was designated as protein Ib, c, 1b and O-8 by different research groups, is functionally and structurally very similar to OmpF. Infrared and CD spectroscopy studies showed that OmpC also has a high content of β structure (Nakamura, 1974). However, these two proteins can be resolved from each other by polyacrylamide gel electrophoresis (Inouye, 1979). There are two differences reported in the sequence of the first 14 amino acids at the N-terminal end (Ichihara and Mizushima, 1978). Most recently, the nucleotide sequence of ompC gene has been reported (Mizuno et al., 1983).

Trimeric OmpC , like trimeric OmpF, forms an aqueous channel which allows small hydrophilic molecules to diffuse across the membrane. The process is also size-selective(Nakae 1976). Nevertheless, the size of the channel formed by trimeric OmpC is slightly smaller than that of the channel formed by trimeric OmpF (Nikaido and Rosenberg, 1983).

Yamada and Mizushima (1980) have isolated OmpC and reconstituted the protein with lipopolysaccharide, lipid A, phospholipid, and fatty acids. These OmpC specimens form two-dimensional periodic arrays with variable center-to-center distances. Grano et al. (1982) studied the structure of negatively stained OmpC specimens, which

had been reconstituted with lipid A. In this study, it was shown that the structure of OmpC is very similar to that of OmpF reported by Dorset et al. (1981).

1.2.5. PhoE

This protein was designated as protein Ic, e, or E and is now called PhoE (Tommassen and Lugtenberg 1980). It is found in E. coli K-12 when the cells are grown under conditions of phosphate starvation. PhoE, OmpC and OmpF all facilitate the diffusion of small hydrophilic molecules. Furthermore, PhoE specializes in the diffusion of negatively charged solutes (Nikaido et al., 1983a; Nikaido and Rosenberg 1983b). The complete nucleotide sequence of the structural gene that codes for PhoE has been reported by Overbeeke et al. (1983). Preliminary structural investigations of negatively stained PhoE have shown that the structure of PhoE is also similar to that of OmpC and OmpF (Jap, personal communication).

1.3. Motivation

The motivation for carrying out the present structural analysis of OmpC by high resolution electron microscopy is developed from asking the following questions.

(a) What is the biological significance of the outer membrane proteins, OmpC in particular, in Gram-negative bacteria?

(b) How does structural information of OmpC relate to the biochemical studies of OmpC?

(c) In the Garavito laboratory, researchers have studied the structure of OmpF by X-ray crystallography. What are the advantages of choosing another line of approach, i.e. electron microscopy, to study the structure of OmpC?

As we have mentioned earlier, structural investigations by electron microscopy have several advantages. We now turn to discuss two major problems encountered in the structural studies of biological specimens by electron microscopy.

CHAPTER 2

Radiation Damage and Specimen Hydration Problems

The structural analysis of biological specimens by high-resolution electron microscopy has encountered two major obstacles: structural damage of the specimen caused by electron irradiation, and difficulty in maintaining specimen hydration in the microscope vacuum. In this chapter, these two problems and various attempts made to overcome them will be reviewed.

2.1. Radiation Damage

The expression "radiation damage" refers to any changes in the physical structure or the chemical makeup of specimens which result from electron beam irradiation. Inelastic scattering between the incident electron and the target atom is the primary cause of radiation damage. However, when the incident electron has a very high energy, elastic scattering can also result in radiation damage.

The inelastic scattering process frequently results in molecular ionization of the specimen. In addition to that caused by molecular ionization, other types of radiation damage, such as specimen etching and effects owing to specimen heating, can also occur.

It is obvious that inelastic scattering will cause radiation damage to the specimen. However, elastic scattering between an incident electron and the nucleus will also cause radiation damage in the form of a displacement of the atom. Owing to the conservation of momentum, the amount of energy transferred to the target nucleus depends upon the kinetic energy of the incident electron and its change in direction after scattering. If the transferred energy is larger than the interatomic bonding energy, then elastic scattering will cause the rupture of the interatomic bond. This type of radiation damage is referred to as atomic displacement and the minimum value of the accelerating voltage to cause atomic displacement is referred to as the threshold voltage.

2.1.1. Molecular Ionization

For biological specimens, molecular ionization can occur in the region of about 5 eV and continue upwards (Glaeser 1979). Molecular ionization will be followed by chemical bond scission, i.e. radiolysis, which may occur on a time scale comparable to the vibrational period of the bond, about 10^{-14} sec.

Quantitative chemical analyses of the radiolysis products show that it is extremely rare for the chemical bond to reform once it is broken. Following radiolysis, the molecular ion fragments and free radicals produced will be

further involved in processes of secondary chemical reactions. The phenomena of the secondary chemical reactions include the formation of carbon-carbon double bonds, cross-linking, chain scission, radical formation and the extrusion of hydrogen atoms.

2.1.2. Specimen Heating

As the amount of energy absorbed by the specimen increases, a well-defined area of localized high temperature is established on the specimen. The extent of the specimen heating depends upon the thermal conductivity of the specimen, the illumination spot size and the electron current density. An approximate relation representing the temperature rise in a thin carbon film irradiated by 100 kV electrons was derived by Grubb and Keller (1972)

$$\Delta T = 0.3 J$$

where J, current density, is expressed in units of Ampere/m^2. In the experiments of low dose electron microscopy, we used a current density ≈ 1 $e^-/Å^2$/min, which is 0.26 Ampere/m^2 (refer to Chapter 3). The calculated temperature rise thus is only ≈ 0.08° C. Therefore, in a high-resolution structural study performed by low dose, low temperature electron microscopy, specimen heating caused by the electron beam is not a primary concern.

2.1.3. Specimen Etching

There is little quantitative information about the specimen etching phenomenon. The phenomenon can only be observed at very high electron exposures, in the range of thousands of electrons/ Å^2, and in the presence of certain residual gasses, such as oxygen and water. Because the electron irradiation needed for specimen etching to occur far exceeds the dose normally used for low dose electron microscopy, specimen etching caused by the electron beam is also not a primary concern in the study of low dose electron microscopy.

2.1.4. Atomic Displacement

The atomic displacement of various atoms is characterized by a threshold voltage. The threshold voltage is proportional to the atomic weight of the target atom and is modified by the strength of the interatomic force. For instance, the threshold voltage for crystalline graphite is over 40 kV in contrast to 27 kV for amorphous carbon (Joy, 1973).

Atomic displacement, occurring as the result of knock-on collisions, is again not a significant factor in radiation damage of biological specimens. It has been shown that for carbon irradiated with 100 kV electrons, the cross section, σ, of knock-on collision is four orders

of magnitude less than that for inelastic scattering (Cosslett, 1978).

2.1.5. Quantitative Measurement of Radiation Damage of the Biological Specimen

In the empirical studies of radiation damage effects, a variety of end points have been used for quantitative measurements of electron radiation damage in thin organic specimens. These included total mass loss, loss of specific elements, loss of crystalline structure, and changes in infrared, visible, ultraviolet, and electron-energy loss spectra. The critical dose is defined as the electron exposure that can be tolerated by the specimen before a specified end point is reached. Much of the experimental work has been reviewed and summarized by Reimer (1965) and Glaeser (1975). At 100 kV, the critical dose for organic molecules composed predominantly of saturated bonds ranges between 0.5 and 5 electron/ $\mathring{A}^2$. However, the critical dose for the molecules with aromatic groups is 5 to 100 times higher than that for the saturated bond molecules. The corresponding figure for phthalocyanine, which is a molecule with extensively conjugated double bonds, is one thousand times higher, i.e. 1200 electron/ $\mathring{A}^2$. More astonishingly, the critical dose of hexadecachlorophthalocyanine, a chlorine-substituted phthalocyanine, is 20 times higher than the parent

molecule (Harada et al., 1972).

In order to express the radiation damage effect in a more quantitative way, it is necessary to know how many molecular fragments are produced for a specific electron dose. This information can be obtained by consulting the radiation chemistry literature to find out the radiolysis yield value, G. The G value is defined as the number of molecules fragmented by the absorption of 100 eV of energy. Unfortunately, radiation biologists and electron microscopists express the dosage in different units. The former uses the term of rads (defined as the deposition of 100 ergs per gram of specimen) and the latter expresses the dosage in the units of electron/$\AA^2$ or coulomb/cm^2, which refer to the number of electrons per unit area irradiating the specimen . It may thus not be obvious that most radiobiological data can be directly compared with results attained by electron microscopy. However, if the amount of energy transferred from the incident electrons to a specimen and the specimen density are known, then it is a very straightforward matter to convert rad to electron/$\AA^2$, and vice versa.

The linear energy transfer value (LET), also referred to as the stopping power, is defined as a statistical average of the amount of energy lost by the primary electron per unit path length within the specimen. For 100 kV

electrons, the LET value is 4×10^{-2} eV Å^{-1} (Stenn and Bahr, 1970). The LET at different accelerating voltages, of the same order of magnitude of 100 kV, is approximately related to the LET at 100 kV by the ratio of $(v_{100} / v)^2$ (Glaeser, 1979), where v is the speed of the accelerated electrons and v_{100} is the speed of the electrons of 100 keV. Once the electron/ Å^2 is converted to rads, we then can search in the literature to find out the radiolysis yield value, G, and estimate the number of molecular fragments produced under the specified electron irradiation. An example is given in the following paragraph.

It is assumed that the accelerating voltage is 100 kV, then LET= 4×10^{-2} eV/Å and electron dose is 1 $e^-/\text{Å}^2$

$$S = \text{LET} \times \text{dose}$$
$$= 4 \times 10^{-2} \text{ eV}/\text{Å}^3$$
$$= 6.4 \times 10^{-14} \text{ erg}/\text{Å}^3$$

where S is the energy per unit volume deposited to the specimen. Let W be the energy per unit mass deposited to the specimen, and d is the density of the specimen, ~ 1 $g/cm^3 = 1 \times 10^{-24}$ $g/\text{Å}^3$, then

$$W = S/d$$
$$= 6.4 \times 10^{10} \text{ erg/g} = 6.4 \times 10^8 \text{ rad}$$

where one rad is defined as the deposition of 100 ergs of energy per gram of mass. For 100 kV electrons, the dose of 1 $e^-/\text{Å}^2$ is equal to 6.4×10^8 rad.

2.1.6. Attempts to Alleviate the Radiation Damage

Several techniques to alleviate the radiation damage will be reviewed in this section. The methodology used to record micrographs in this thesis project combines some of these techniques to minimize the radiation damage effect to the specimen. The detailed procedure of the methodology will discussed in Chapter 3.

A. Minimal Exposure Technique

A minimal exposure is one for which the specimen is exposed to the electron beam only when an image of the specimen is being recorded. The success of this technique was demonstrated in imaging negatively stained Tobacco Mosaic Virus (TMV) particles (Williams and Fisher,1970a), T-4 bacteriophage (Williams and Fisher,1970b) and the oligomeric enzyme, Aspartate Transcarbamoylase (ATCase) (Richards and Williams,1972). The micrographs obtained with this technique show clearly the helical structure of the TMV particle with a pitch of 23 Å, the morphological features in the tail structure of the T-4 bacteriophage and the triangular arrangement of the catalytic subunits of the ATCase molecule. However, the prerequisite for applying this technique is that the specimen distribution on the EM grid be very homogeneous.

Even under minimal exposure conditions, some considerable radiation damage still occurs. In practice, the useful resolution obtained with this minimal exposure technique for stained specimens does not go much beyond 15 Å to 20 Å. This is because the dose used for recording a micrograph with the minimal exposure technique, at a magnification of 40,000, is about 16 electron/ $Å^2$, while the structural features in the range of 5 to 10 Å are pretty much destroyed at a dose of 1 to 10 electron/ $Å^2$ (Glaeser 1979).

B. Low Dose Electron Microscopy

It is apparent that micrographs containing high-resolution structural information of the biological specimens must be obtained with an exposure that is under the critical dose of biological specimens. Under this condition, the minimal object size that can be seen on the micrograph is limited by the statistical nature of electron events on the micrograph. The quantitative relationship between the resolution, the contrast of the specimen and the critical dose of the specimen is given by the Rose equation (Glaeser, 1971)

$$d\,C \geq \frac{5}{(fN_{cr})^{1/2}}$$

where d is the minimal object size to be seen, C is the contrast of the object relative to the surrounding, f is the detection efficiency of the recording medium, and N_{cr}

is the critical dose of the specimen. Let f become a maximum, unity; C is typically 0.1 in bright field images of biological specimens; and $N_{cr} \approx 1$ electron/ $\mathring{A}^2$. It is thus easy to calculate that the minimal size of the object that can be seen with confidence is ≈ 50 $\mathring{A}$.

However, if some prior knowledge of the object is available, high-resolution structural information about the object is still retrievable. (Mathematically speaking, we reduce "5" in the Rose equation to a smaller value.) For example, in the structural study of proteins in a 2-D periodic array, our prior knowledge indicates that the structure is composed of unit cells at a fixed separation and in identical orientations. Using this information, it is possible to record a micrograph of a crystalline specimen with a dose that is well below the critical dose and then to superimpose unit cells on top of each other with the result that the signal-to-noise ratio of the micrograph will increase as the process continues. This technique, known as the spatial averaging technique of structure determination by electron microscopy of unstained, crystalline biological specimen (Kuo and Glaeser, 1975), has been successfully applied to the high-resolution structural study of bacteriorhodopsin in the membrane of Halobacterium halobium (Henderson and Unwin, 1975; Unwin and Henderson, 1975; Hayward et al.,

1978). Today, this spatial averaging technique has become a part of standard procedure of low dose electron microscopy.

C. High Voltage Electron Microscope (HVEM)

The rationale for using high accelerating voltages, such as 1 MeV or more in HVEM, to circumvent radiation damage is that the LET value of the incident electrons will thereby decrease. It has been reported that an increase in voltage from 80 to 500 kV is accompanied by a significant reduction of damage in crystals of l-valine (Glaeser, 1971). However, for thin organic specimens, the critical dose for a specified end point, such as in the case of complete loss of the electron diffraction pattern, does not change with respect to the accelerating voltage in exactly the same way as does LET (Howitt et al., 1976). The critical dose depends on β^3 rather than β^2 as predicted from stopping power theory, where $\beta = v/c$, the ratio of the speed of the electron to that of light.

In addition to reduction of the radiation damage to the specimen, HVEM also has a higher resolving power because the limiting resolution value is proportional to $C_s^{1/4}\lambda^{3/4}$, where C_s is the spherical aberration coefficient of the objective lens and λ is the electron wavelength. This advantage will improve the visibility of the specimen such that a lower electron dose can be used.

Therefore, less radiation damage is done to the specimen.

D. Image Intensification

The idea of using an image intensifier to alleviate radiation damage results from a failure to understand the nature of the limitation of the image detectibility. The image intensifier could serve as a better recording device only if it could increase the value of the detection efficiency f in the Rose equation. However, it has been found that the Kodak Electron Image Plate (EIP) has a superior electron detection efficiency to the existing TV system (Kuo and Glaeser,1975). Better intensifiers can be built (Herrmann et al.,1978); nevertheless, the theoretically attainable improvement is small.

E. Low Temperature Electron Microscopy

A thorough review of radiation damage of biological specimens at low temperature has been done by Glaeser and Taylor (1978). Radiation damage will be reduced substantially when the specimen is at low temperature. It is generally believed that, at low temperature, secondary chemical reactions have less opportunity to occur, following the primary radiolysis. At low temperature, the cage effect provided by the neighboring molecules restricts the diffusion of the reactive species and therefore limits the secondary chemical reactions. Meanwhile, some chemical

reactions which need large activation energy might not happen at a low temperature.

It has been shown that, at -120° C, the electron exposure required to completely destroy the electron diffraction pattern of frozen hydrated catalase is about 18 electron/$\AA^2$, which is about 10 times greater than the corresponding figure found for wet hydrated catalase at room temperature (Taylor and Glaeser,1976). It has also been shown that the critical dose of the purple membrane increases by at least a factor of 4 when the specimen is maintained at ≈ -120° C (Hayward and Glaeser, 1979). At the present time, there is no strong evidence to show advantages of operating the microscope under liquid helium temperature versus liquid nitrogen temperature, in terms of increasing the radiation damage protection for biological specimens.

Low temperature electron microscopy offers another important advantage: to overcome the difficulty in maintaining specimen hydration. This aspect will be reviewed in the next section.

2.2. Specimen Hydration Problem

When the natural aqueous environment of a biological specimen is replaced by the high vacuum of the electron microscope, the vacuum dehydrates the specimens, thus

causing damage to their structures. In this section, several methods of specimen preparation that have been developed will be discussed. In addition, techniques which have been developed in this laboratory to prepare frozen hydrated specimens for low temperature electron microscopy will be discussed.

To evaluate each method, we will use the electron diffraction patterns of protein crystals to indicate the extent of the specimen preservation. It is believed that maintaining the crystallinity of the specimen is a sufficient condition for preserving the individual molecules of the specimen. Furthermore, specimen crystallinity is essential for carrying out high resolution structure analysis by low dose electron microscopy. Therefore, whether the specimens remain in the crystalline form when they are in the microscope is of primary concern.

2.2.1. Air-Drying

Owing to the extreme pressure exerted by the surface-tension effect, three dimensional objects prepared by a simple air-drying process will be pressed flat into the support film. It has been calculated that the stress through a bacterial flagellum is 46,000 kg/cm ^{2} (Anderson,1956). Thus, so far as we know, no single-crystal electron diffraction pattern of bR has ever been obtained from specimens that were prepared using this method.

However, electron diffraction powder patterns of bR can be obtained by the air-drying method, if bR membranes are air-dried with several layers of membranes stacked on top of each other.

Critical point drying and freeze drying are two alternative methods for specimen preparation. They both circumvent the need to pass the specimen through the liquid-gas phase transition of the ambient liquid during the drying process. Both techniques have been described in detail by Boyde and Wood (1969).

2.2.2. Critical-Point Drying

"Critical point" refers to the combination of a critical temperature, T_c, and a critical pressure, P_c, of the system such that the density of the vapor and of the liquid are identical. Under these circumstances, the liquid-gas phase transition disappears and the surface tension is zero.

In this drying process, water in the biological specimen is replaced with liquid carbon dioxide or liquid freon, because the T_c and the P_c of H_2O, 374^{o} C and 217.7 atm respectively, are too high for practical purposes. In contrast, the corresponding figures, for CO_2 are 31.2^{o} C and 72.8 atm. Since liquid CO_2 is immiscible with H_2O, H_2O is first replaced by ethanol, then by amyl alcohol,

and finally the amyl alcohol is replaced by liquid CO_2. The specimen is first immersed in the liquid which is below the critical temperature, then, the system is carried through the critical point to a temperature above the critical temperature. Thus, the specimen dries without ever having passed through the liquid-gas interphase.

The critical-point drying technique has been widely used in the field of scanning electron microscopy. It is useful particularly with larger objects such as unicellular organisms and small animal and plant tissues. However, it has been observed that fibrous structure collapsed onto the support film after critical-point drying (Anderson,1954). In addition, ethanol and amyl alcohol are potent reagents for denaturing proteins and for extracting lipids from membranes. Therefore, this technique is of little use for high-resolution structural studies of membrane proteins.

2.2.3. Freeze-Drying

Wyckoff was probably the first who tried to freeze-dry viruses on a grid (Wyckoff, 1946). Williams, a few years later,introduced a more sophisticated and more reliable device for freeze-drying red blood cell ghosts, DNA and T-bacteriophages (Williams 1952,1953; Williams and Fraser,1953). The freeze-drying technique involves quickly freezing the specimen in such a way as to avoid

ice crystal formation. The frozen specimen is then transferred as quickly as possible onto a pre-cooled (-150° C) specimen stage. The chamber is then evacuated, while the stage gradually warms up to room temperature. As a result all the ice sublimes and the specimen dries.

Freeze-drying preserves the structural information of specimens at intermediate resolution, but not at high resolution. This has been demonstrated in the freeze-drying and shadowing of a two dimensional crystalline specimen, in vitro reassembled T-layer cylinders from the outermost protein layer of Bacillus brevis (Kistler et al.,1977). The highest diffraction order in the optical diffraction patterns of the images of such specimens corresponds to a resolution of ~25 Å. However, the low-angle X-ray diffraction pattern of wet, hydrated specimens showed the initial specimen order was about 15 Å. Freeze-dried catalase crystals on the other hand produced electron diffraction patterns out to 8.5 Å, in contrast to 3.4 Å obtained from frozen hydrated catalase crystals (Lepault and Dubochet,1980)

2.2.4. Negative Staining

Negative staining techniques were first used to increase specimen contrast. The staining reagents commonly used, depending upon specimens, are phosphotungstate, uranyl acetate, uranyl formate, etc. The reagents

replace the H_2O in the specimen while it is air-dried. As a result of this replacement, for example, an electron dense core exists in the center of a negatively stained TMV particle. The phenomenon of the staining reagent occupying water channels has been demonstrated most elegantly by recent work in which negatively stained catalase crystals were subsequently embedded in epon and sectioned. Water channels filled with uranyl acetate can be seen clearly (Jésior, 1982).

The highest electron diffraction order of negatively stained specimens is usually limited to a resolution of 15~20 Å. This should not be attributed to the grain size of staining particles. Instead, it is due to many different factors, not the least of which are the drastic increase of both the ionic strength and the pH value of the surrounding media while the specimen is air-dried.

The negative-staining technique will increase the critical dose of the specimen at a resolution of 25~35 Å. However, changes in intensity distribution of the diffraction pattern have been observed as a function of electron exposure, even at this relatively poor resolution (Glaeser, 1971). This result confirms the suggestion that under electron irradiation, the staining reagents redistribute themselves within each unit cell. This redistribution is evidently identical within each unit cell on a

size scale of 25 Å or more. Nevertheless, the typical electron irradiation on the stained specimen which causes such effects is about 100 electrons/Å^2 (Glaeser, 1971). Therefore, the reliability of the structural information obtained from minimal exposure techniques, which involve a dose of only 15 to 20 electrons/ Å^2, should not be questioned.

2.2.5. The History of Specimen Hydration Efforts

Since the invention of the electron microscope, several attempts have been made to observe living materials in a hydrated state. Various kinds of environmental chambers, which separate the specimen from the microscope vacuum thus keeping the specimen hydrated, have been developed for this purpose. A brief review of various approaches was reported by Fullam (1972).

Most early designs of environmental chamber involved the use of thin-film windows, which allowed electrons to penetrate but prohibited water vapor from escaping. The disadvantages of these approaches are: (a) the windows, which experienced both a tremendous pressure difference on both sides of the film and severe electron bombardment, always proved to be very fragile; (b) as a result of the strong electron scattering by the windows, the images are of low contrast. Even with the aid of a high voltage electron microscope, the outcome of observation of wet

biological specimens is not encouraging (Nagata and Ishikawa, 1972).

A new design using a differentially pumped environmental chamber produced electron diffraction patterns of wet catalase crystals with reflections of up to 2 Å resolution (Matricardi et al., 1972). The chamber consists of four collinear apertures through which the electron beam passes. A pressure gradient is maintained across the apertures by constantly feeding the specimen with water vapor and differentially pumping the low-pressure side of the apertures. Because of the size of the environmental chamber, images have to be recorded with a long focal length of the objective lens.

Although this approach has resulted in great success in recording electron diffraction patterns, it presents some disadvantages which make it difficult to apply to the thesis project. The major disadvantages are: (a) the spherical aberration arising from the long focal length of the objective lens and the inelastic scattering caused by the water vapor inside the chamber make it difficult to obtain high resolution images, (b) the difficulty of adequately controlling the rate of feeding water vapor, so that either rapid water condensation or evaporation will occur. Therefore, the use of the environmental chambers to protect specimens from dehydration is not practical, and

another line of approach has to be investigated.

2.2.6. Glucose Embedding

Another way to solve the specimen hydration problem is to replace the aqueous medium by another medium which has similar chemical and physical properties, but is non-volatile. Using glucose as the substituting medium, Unwin and Henderson have determined the projected structures of unstained catalase and bacteriorhodopsin (bR) at a resolution of 9 Å and 7 Å respectively (Unwin and Henderson, 1975). The three dimensional structure of glucose-embedded bR, at a resolution of 7Å x 7Å x 14Å, has also been determined (Henderson and Unwin,1975). Micrographs of glucose-embedded bR recorded at liquid nitrogen temperature and then analyzed with the phase refinement method (by assessing the probability distribution) at each reflection has shown structural information at a resolution of 3.7 Å (Hayward and Stroud, 1981).

The glucose-embedding technique is certainly convenient. However, the density of glucose is close to that of protein, and it is thus sometimes difficult to interpret the map. This may be the reason why there is no significant signal shown on the difference Fourier map between C-terminus cleaved bR and native bR (Wallace and Henderson, 1981).

2.2.7. Frozen-Hydrated Specimen Preparation

This technique involves quickly freezing the specimen and then rapidly transferring the frozen specimen into the microscope. The specimen remains at a low temperature, -120°C, during examination. Electron diffraction patterns and high contrast images of frozen hydrated catalase have been obtained with this method (Taylor and Glaeser, 1974). The diffraction pattern shows the highest reflection order at a resolution of 3.4 Å. Recently, electron diffraction patterns of frozen hydrated bR have been obtained which show the highest reflection order at a resolution of 3.2 Å (Jaffe and Glaeser, 1982).

As mentioned in the previous section, this method allows the critical dose for the high resolution reflection to increase 3 to 10 times. The statistical definition of the image is thereby enhanced. However, the amount of water remaining on the EM grid just before it is immersed in liquid nitrogen becomes very crucial; the layer of water has to be thin enough to allow electrons to pass through, yet, thick enough to maintain the specimen in a hydrated state. Two methods by which Taylor and Glaeser tried to control the optimal thickness of the water were: (1) to sandwich the specimen between two carbon-coated folding grids, and to squeeze out the bulk water by tightening the folding grids; (2) to slow down

water evaporation by performing the specimen preparation in a humidity box, and to judge the water thickness in a phase contrast light microscope by watching the interference fringes which are produced from the bulk water on the EM grid. Neither method was fully satisfactory in terms of giving reproducible results.

In this laboratory, two further methods were developed to circumvent this problem. One of them is referred to as the double-carbon film method (Jaffe and Glaeser, 1982). A general description of this technique is presented as follows. Carbon is first evaporated onto a mica platelet to form a carbon film. The film is then floated on distilled water. A precleaned EM grid is submerged in the distilled water and lifted through the carbon film. After the surface of the grid has dried, the specimen is applied onto the grid. After an appropriate time the grid is immersed into the distilled water again, and the excess specimen is thus rinsed off. Finally, the grid is lifted through the carbon film once again. After waiting for the excess water to evaporate from between the carbon films, the grid is subsequently plunged into liquid nitrogen at the proper time, which is judged by watching the color changes of the grid during the water evaporation. If it happens that the specimen does not adhere to the grid well, then the specimen can be deposited onto the

grid by centrifugation. This modification to the double-carbon method proved to be very successful (Sosinsky, 1983). The double-carbon film method is quick and simple; however, it is not applicable to specimens which have to be in a buffer or in a solution containing specific ions. The distilled water can be replaced by the specific buffer; nevertheless, the ionic strength will become too high when the sandwiched "bulk water" evaporates.

The other technique, the fatty-acid monolayer method, is expected to be applicable to many specimens. This technique involves squeezing the bulk water out by the fatty-acid monolayer, through the electro-static interaction between the monolayer and a layer of poly-lysine, which has been deposited on the surface of the grid. In Chapter 3, this method will be described in detail.

CHAPTER 3

Techniques of Frozen-Hydrated Specimen Preparation and Low Dose Electron Microscopy

In the previous chapter, it has been shown that high-resolution structural information is obtainable for specimens only if they are in a fully hydrated state and that the use of frozen-hydrated specimens had many advantages in this regard. However, early techniques for preparing frozen-hydrated specimens either had difficult-to-control results or were not applicable to specimens requiring maintaining a buffer with a specific ionic strength or pH value. In this chapter, we shall discuss a new preparation technique for frozen-hydrated specimens: the fatty acid monolayer technique. In addition, we shall describe the techniques for recording low dose electron diffraction patterns and for obtaining low dose images. The structural investigation of frozen-hydrated OmpC will be discussed in the next chapter.

3.1. Background

In chapter 2, we mentioned that the double-carbon film technique developed by Jaffe worked successfully in preserving the specimen in a frozen hydrated state. However, this technique has two major flaws: (a) A non-uniform layer of water forms across the EM grid when the grid is frozen. Specimens in areas containing thick ice

cannot be recorded because the electrons are unable to penetrate the ice. On the other hand, specimens in areas containing no ice are air-dried and, therefore, cannot maintain their crystallinity. (b) After the second layer of the carbon film is picked up, a droplet of solution is sandwiched between the two carbon layers. If the solution contains a specific ion concentration and pH value, these values will drastically change during evaporation of the solution.

The fatty acid monolayer technique, developed by Hayward et al (1978), involves depositing a polylysine monolayer on an EM grid. The grid is then withdrawn through a monolayer of stearic acid, $CH_3(CH_2)_{18}COOH$. The electrostatic charge-charge interactions between these two monolayers expel the bulk water from the grid. However, the stearic acid monolayer can expel the bulk water only when two conditions are met: the solution contains a high concentration of Ca^{+2} and has a high pH. This condition is not suitable for most biological specimens.

3.2. Method

We have developed a new version of the fatty-acid monolayer technique in order to increase the extent of the "usable" specimen on the EM grid and to provide a technique which can be applied to many biological specimens. This technique is derived from the method, which was first

reported by Blodgett (1935), for depositing a stearic acid monolayer on a solid surface. Waldbillig et al.(1976) reported that a behenic acid monolayer can also be deposited on solid surfaces in distilled water. In this thesis study, behenic acid, $CH_3(CH_2)_{20}COOH$, has been used and has been shown to adhere to suitably prepared EM grids, as they are withdrawn from a subphase of distilled water.

The specimen preparation procedure is described in the following paragraphs. A formvar film is floated onto distilled water, and four 200-mesh EM grids are dropped onto the film. A plastic coverslip is then laid onto the formvar film. The EM grids are thereby sandwiched between the formvar film and the coverslip. This formvar-grid-coverslip complex prevents water from reaching the back side of the grid. Next the coverslip is picked up, air-dried, and then evaporated with a few hundred Å of carbon. These carbon-coated coverslips are stored in a dessicator to keep them away from surfactants.

Several steps are required prior to freezing the specimen. The coverslip is glow-discharged for 60 sec with an AC voltage of 0.8 kV under a vacuum of 120 milli-torr. The surface of the coverslip complex is subsequently treated with a few droplets of polylysine solution (5 mg/ml). Two to five minutes later, the coverslip is rinsed vigorously with distilled water. If the surface of

the coverslip is hydrophilic, interference fringes arising from the drying of the bulk water will be observed everywhere on the surface.

About 2µl of the sample solution are then applied to each of the EM grids. After three minutes, the coverslip is rinsed off with distilled water, and is submerged in a precleaned crystallizing dish containing distilled water. The dish is put in a water bath to maintain the subphase at a temperature of ~ 30° C.

A drop of castor oil is applied to the water surface. The oil will spread out uniformly until it reaches the wall. Castor oil serves as a "piston" to compress the behenic acid molecules into a closely packed arrangement. A droplet of ~0.05% behenic acid in distilled hexane is then applied onto the castor oil film. The behenic acid solution has also been warmed to a temperature ~ 30° C. The behenic acid will compress the castor oil film into small lenses. Within a minute, the hexane evaporates and the behenic acid forms a rigid monolayer film on the water surface. The coverslip is then withdrawn slowly and steadily through the behenic acid layer. The surface of the EM grids should appear to have no bulk water. A schematic diagram of the specimen preparation is shown in Fig. 3.1.

Fig. 3.1 A schematic drawing of the adherence of the behenic acid monolayer to a polylysine-coated coverslip when it is withdrawn from the subphase of water.

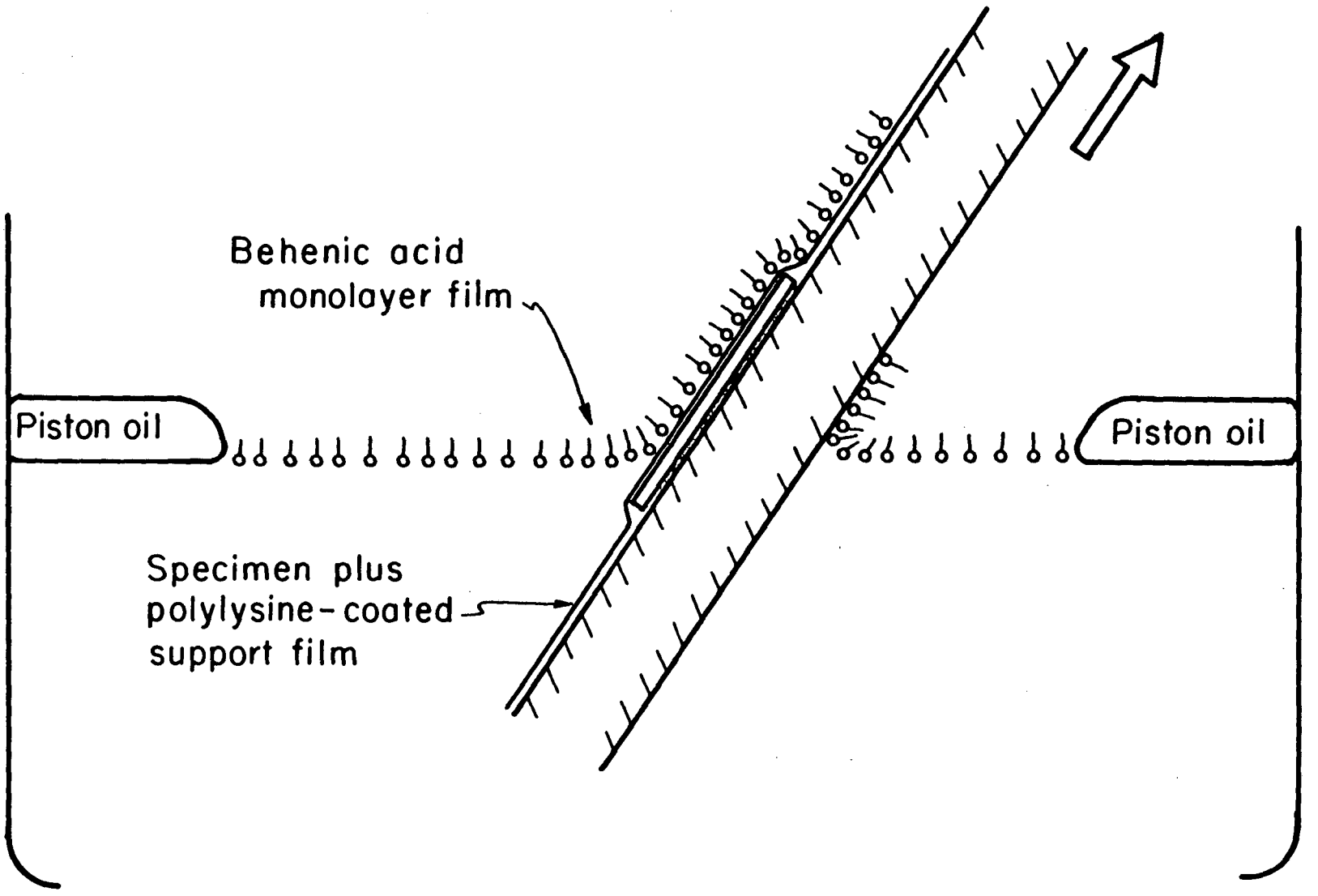
Behenic acid
monolayer film
Piston oil
Piston oil
Specimen plus
polylysine-coated
support film

XBL822-3635

One of the grids is removed from the coverslip and frozen immediately in liquid nitrogen. The grid is then mounted onto a specimen-holder cartridge under the liquid nitrogen. Through a transfer device (Taylor and Glaeser, 1975), the cartridge is then transferred immediately into the microscope stage, which has been precooled to ~-125°C. The stage temperature is maintained at ~-125°C throughout the time span of the experiment.

3.3. Results

We chose bacteriorhodopsin (bR) as a test specimen for this monolayer technique of specimen preparation. The bR specimens, which were obtained from Dr. Stoekenius' laboratory, had been isolated from an R1 strain of *H. halobium*.

3.3.1. Electron Diffraction of Frozen-Hydrated bR

Low dose electron diffraction patterns of frozen-hydrated bR were recorded using Kodak X-ray AA Film. The instrument used was a JEOL 100B electron microscope, equipped with a cold stage which was built in this laboratory (Hayward and Glaeser, 1980). The stage temperature was monitored by means of a thermo-couple.

A high-contrast specimen holder was used in this diffraction study. Specimens were scanned at a low magnification by overfocusing the intermediate lens in diffraction

mode. The advantages of this operation are two fold: the contrast of the specimen is enormously high, and the illumination and the magnification on the viewing screen can be adjusted in an optimal combination at the user's will. The electron dose rate on the specimen was ~ 1 electron/Å^2/min. The procedure for recording low dose electron diffraction patterns is described below.

Once a promising membrane patch is found, a smaller condenser aperture is inserted into the pathway of the electron beam. The size of the condenser aperture is chosen such that the electron beam illuminates only this membrane patch or a part of it. In this study, the appropriate size of the illuminated area is ~0.25μm^2. The diffraction patterns are obtained by re-focusing the intermediate lens. The exposure time used to record the electron diffraction patterns is ~90 to 150 seconds. The total electron dose received by the specimen producing the diffraction pattern is therefore ~1.5-2.5 electron/Å^2.

In our electron diffraction experiments, exposed AA films were developed in Kodak KLX x-ray film developer for 8 minutes. With the combination of the patch size chosen and the electron dose used to record the pattern, this process produces electron diffraction patterns with an appropriate optical density.

An electron diffraction pattern of frozen-hydrated bR prepared by the monolayer technique, Fig. 3.2, shows the highest reflection orders at a resolution ~ 7 Å. Six-fold, diffuse, behenic acid diffraction spots are visible in the original film. This result provides validation that the behenic acid monolayer technique maintains high-resolution structural information of the crystalline structure of bR.

3.3.2. Low Dose Images of Frozen-Hydrated bR

Low dose electron micrographs of frozen-hydrated bR were recorded, at a magnification of 40,000, using Kodak Electron Image Film. The procedure for recording low dose images is a modified version of the minimal exposure technique (Williams and Fisher, 1970).

In our microscope, there are three independent controls that can be used to vary the lens current of C2. The electron dose rate can be preset at three different values. One is used for scanning the specimen, and is set at a dose rate of 1 $e^-/Å^2$/min; another is used for recording micrographs, and is set at a dose rate of 300 $e^-/Å^2$/min; and the third is used for focusing the image at magnifications of approximately 40,000. In setting up the C2 current for focusing the image, the electron beam is converged into a small crossover of ~ 0.5μm diameter with a sufficiently high dose rate that the focus-dependent

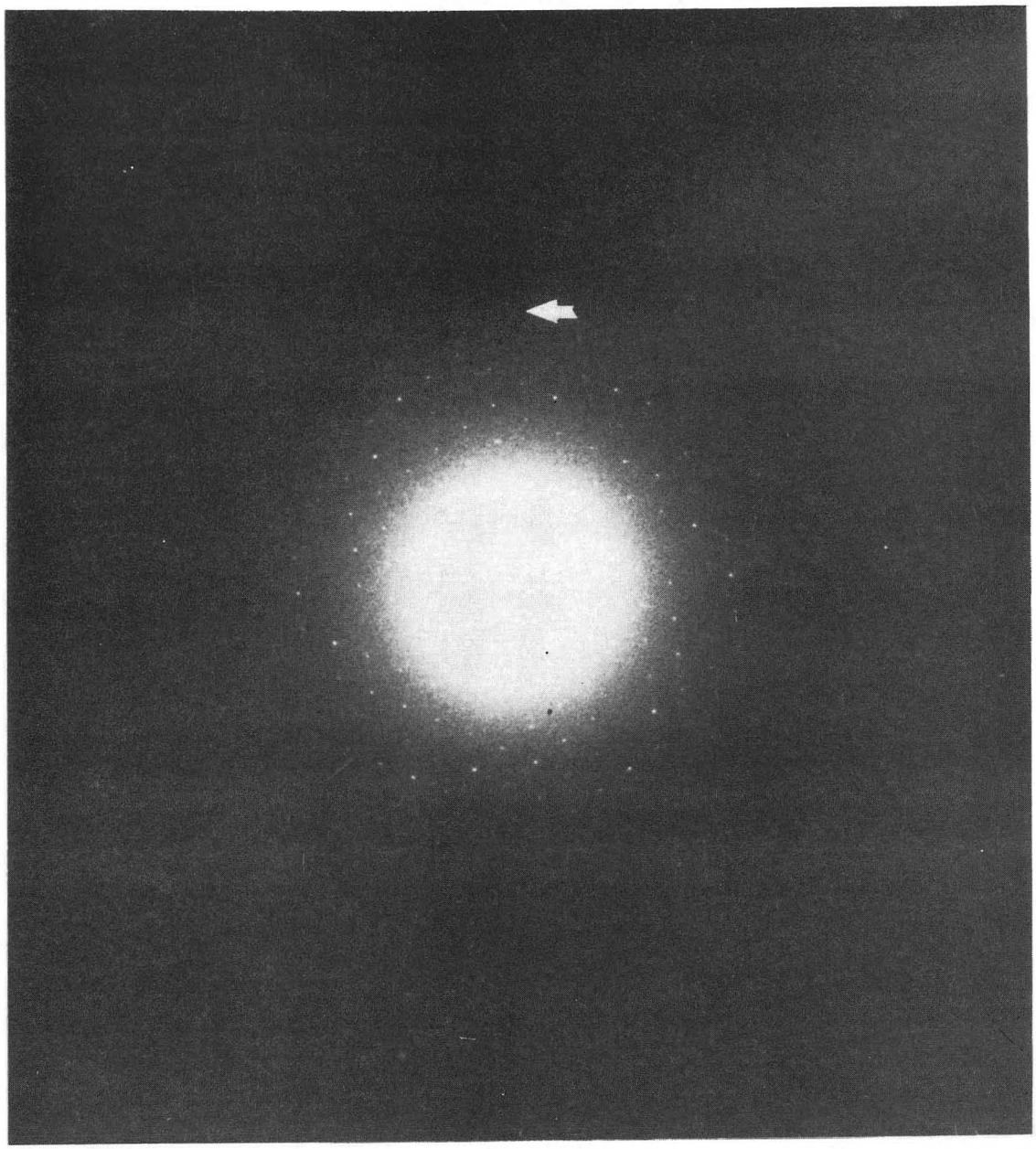

XBB 835-4440

Fig. 3.2 Electron diffraction pattern of bacteriorhodopsin. The highest reflection order shown by the arrow corresponds to a resolution of ~ 7 Å.

phase contrast granularity is readily visible.

There is also a shutter system built into our microscope, which is used to minimize the structural damage of the specimen arising from unnecessary electron irradiation. The shutter system employs a deflection coil near the field emission gun. The coil deflects the beam off the anode aperture so that the electron beam will not enter the condenser lens system and illuminate the grid. Whenever we vary the different settings of electron dose rate, we close the shutter such that the the areas which have not been scanned cannot be illuminated. The structural damage within the specimen arising from electron irradiation thereby remains minimal. The procedure for recording low dose electron micrographs uses the beam shutter and the three preset illumination conditions, which are described below.

In low dose imaging, we first set up the voltage-axis alignment and objective lens astigmatism correction, both when the beam position is controlled by the bright field settings of the deflection coil system in the condenser lens and when the beam position is controlled by the "dark field" settings of same system. The dark field controls are actually used to produce a normal bright field image, but the translation knobs in the dark field system are used to deflect the electron beam so that the beam

illuminates a small fluorescent screen that is mounted in front of the standard viewing screen.

Specimens are scanned in the same way as described in the previous section. At this point, the electron dose rate received by the specimen is ≈ 1 electron/Å^2/min. When promising membrane patches are found, we close the shutter and switch to the dark field setting so that the electron beam will subsequently illuminate the front fluorescent screen. Meanwhile, we switch to the C2 control which has been preset to converge the electron beam into a crossover. Under these conditions, the area for which the low dose image will be recorded is not irradiated by the electron beam. We switch the electron microscope operation mode from the diffraction mode to the image mode and then open the shutter. An area next to the specimen can then be brought into the desired focus at a magnification of 40,000.

After an appropriate focusing value is set, we close the shutter and switch to the C2 control which has been preset to produce an electron dose rate of ~300 electron/Å^2/min. In addition, we switch back to the bright field setting and open the shutter. The low dose image is recorded for an exposure time of 1 sec. The total electron dose to the specimen for recording low dose images is ~5 electron/Å^2.

A low dose image of frozen-hydrated bR and the optical diffraction pattern from this image are shown in Fig. 3.3. The whole bR membrane patch covers almost the entire micrograph and its size is estimated to be ~ 1.5 μm in diameter. The membrane patches in this Figure are almost invisible, although a folded area in the region of the circle is darker and somewhat easier to see. The optical diffraction pattern from the circled area shows that the highest reflection order corresponds to structural information of bR at a resolution of ~10 Å. Since the circled area is actually a fold in the membrane, the diffraction pattern shows crystalline domains with more than one orientation.

The purpose of performing these studies was to assess the success of specimen preservation by the fatty acid monolayer technique. Quantitative data analysis was not performed for the bR specimens. However, a qualitative comparison of the intensity of diffraction spots, corresponding to a resolution of 10 Å, with their neighboring background indicates that the signal-to-noise ratio of these reflections is fairly high.

3.4 Discussion

A major disadvantage of the fatty acid monolayer technique is that the process of preparing the grid has to be carefully executed at every step (from the glow-

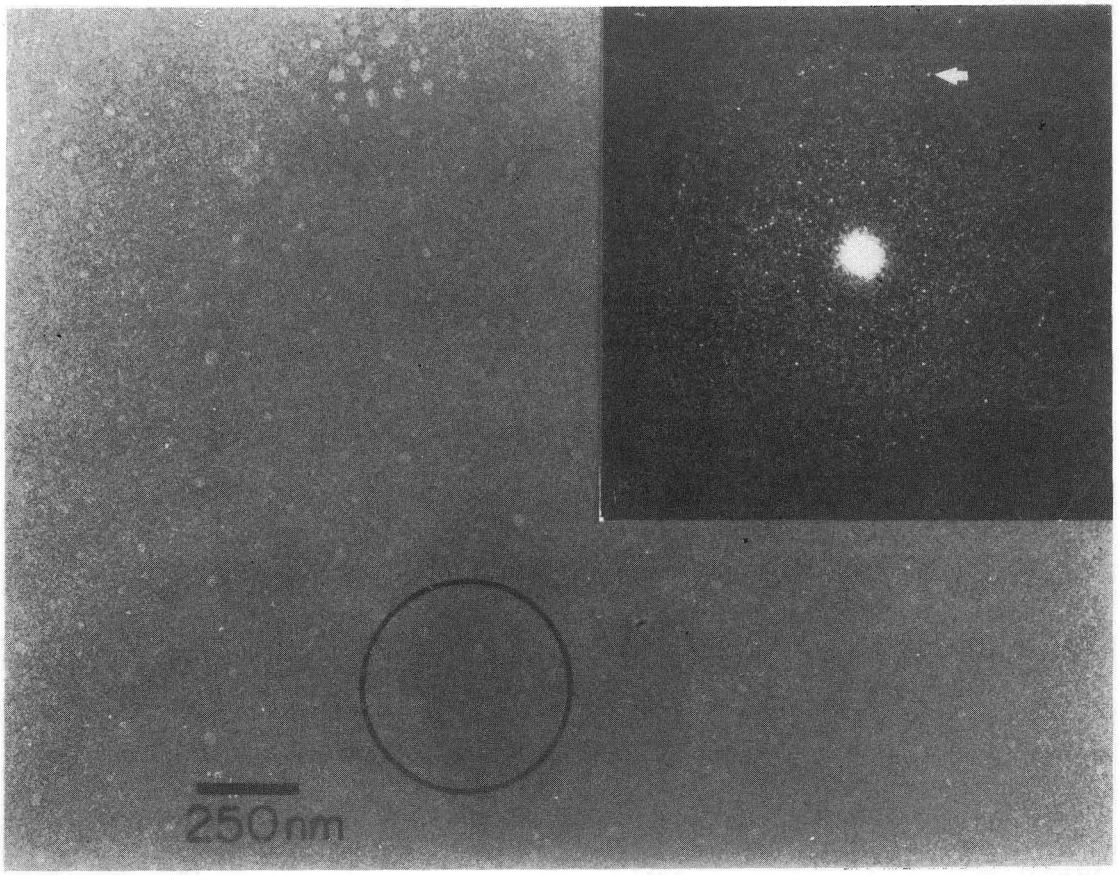

XBB 833-2079

Fig. 3.3 Low dose image of bacteriorhodopsin and its optical diffraction pattern. The highest reflection order, indicated by the arrow, corresponds to a resolution of ~ 10 Å.

discharge treatment of the grid to pulling it through the monolayer prior to freezing). The surface of the grid has to be surfactant-free at all times. If the surface becomes hydrophobic at any point in the process, then that grid or coverslip must be discarded. This fact will quickly exhaust the user's patience. However, if one can control the parameters mentioned in the following paragraph then this technique will provide successful results.

By trial and experience, I have found that: (a) The time of glow-discharge treatment of the grid has to be ~ 60 sec with an AC voltage of 0.8 kV; otherwise, the surface of the grid will not be hydrophilic. For example, after a 30 sec glow-discharge time, water droplets will still form on the surface of the coverslip when the polylysine is rinsed off. (b) The surface of the grid can be contaminated by surfactants from the tips of the forceps. Therefore, the forceps should be washed with detergent and then rinsed with alcohol before being used to hold the grid. (c) The crystallizing dish has to be washed very thoroughly. This can be achieved by first washing the dish with detergent and then rinsing it with hot tap water. Finally, the dish is rinsed thoroughly with distilled water.

Only specimens which are covered by the behenic acid layer produce electron diffraction patterns; every elec-

tron diffraction pattern of bR is therefore accompanied by an electron diffraction pattern of behenic acid. In fact, one can observe the six-fold electron diffraction spots of behenic acid on the fluorescent screen when the smaller aperture is inserted into the electron pathway. Only if the diffraction spots can be seen on the screen do we record the diffraction pattern of bR.

The adherence of the monolayer to the coverslip may not be successful depending upon the density of the sample coverage on the grid and the negativity of the sample surface which is exposed to the aqueous environment. If it is the case, another layer of polylysine should be applied in order to overcome the difficulty. This modification worked successfully for preparing frozen-hydrated OmpC specimens, which will be discussed in Chapter 4.

The fatty acid monolayer technique has not yet been tested for preparation of frozen specimens in solutions with a specific ion concentration and pH value. However, the technique involves trapping a thin layer of water just prior to the time when the grid is frozen. There is little water evaporation. The dramatic change of ion concentration and pH which occurs in the double-carbon film method is not expected to occur with the fatty acid monolayer technique. If the solution has a very high concentration of ions, then it is likely that the adherence of

the behenic acid monolayer to the polylysine layer might work poorly, due to electrostatic shielding by the ions in solution.

The fatty acid monolayer technique for preparation of frozen-hydrated specimens successfully preserves the high-resolution structural information of bR. In the next chapter, I will discuss the application of this specimen preparation technique to another biological system: the outer membrane protein OmpC.

CHAPTER 4

Structural Analysis of Frozen-Hydrated OmpC

In Chapter 3, it was shown that frozen-hydrated purple membranes can be successfully prepared by applying the behenic acid monolayer technique. In this chapter, we will discuss the structural analysis of the projection of frozen hydrated two-dimensional crystals of OmpC prepared using the same technique. We will also present and compare the results of the structural analysis of the projection of the same specimen which was stained. The comparison between these two results provides insight regarding the three-dimensional topology of the OmpC molecule.

4.1 Materials and Methods

4.1.1. OmpC Isolation and OmpC-Lipid A Reconstitution

The OmpC specimens that we have studied were kindly provided by Professor S. Mizushima of Nagoya University, Japan. These specimens were prepared by reconstituting purified OmpC protein with Lipid A. The outer membrane protein, OmpC, was isolated from a mutant strain of *E. coli* K-12, named *E. coli* YA21 (K-12, F^- met leu λ^-). Procedures for bacterial growth and protein isolation have been described in detail by Nakamura and Mizushima (1976). A schematic diagram depicting the procedure of OmpC isolation and purification is shown in Fig. 4.1. A member of

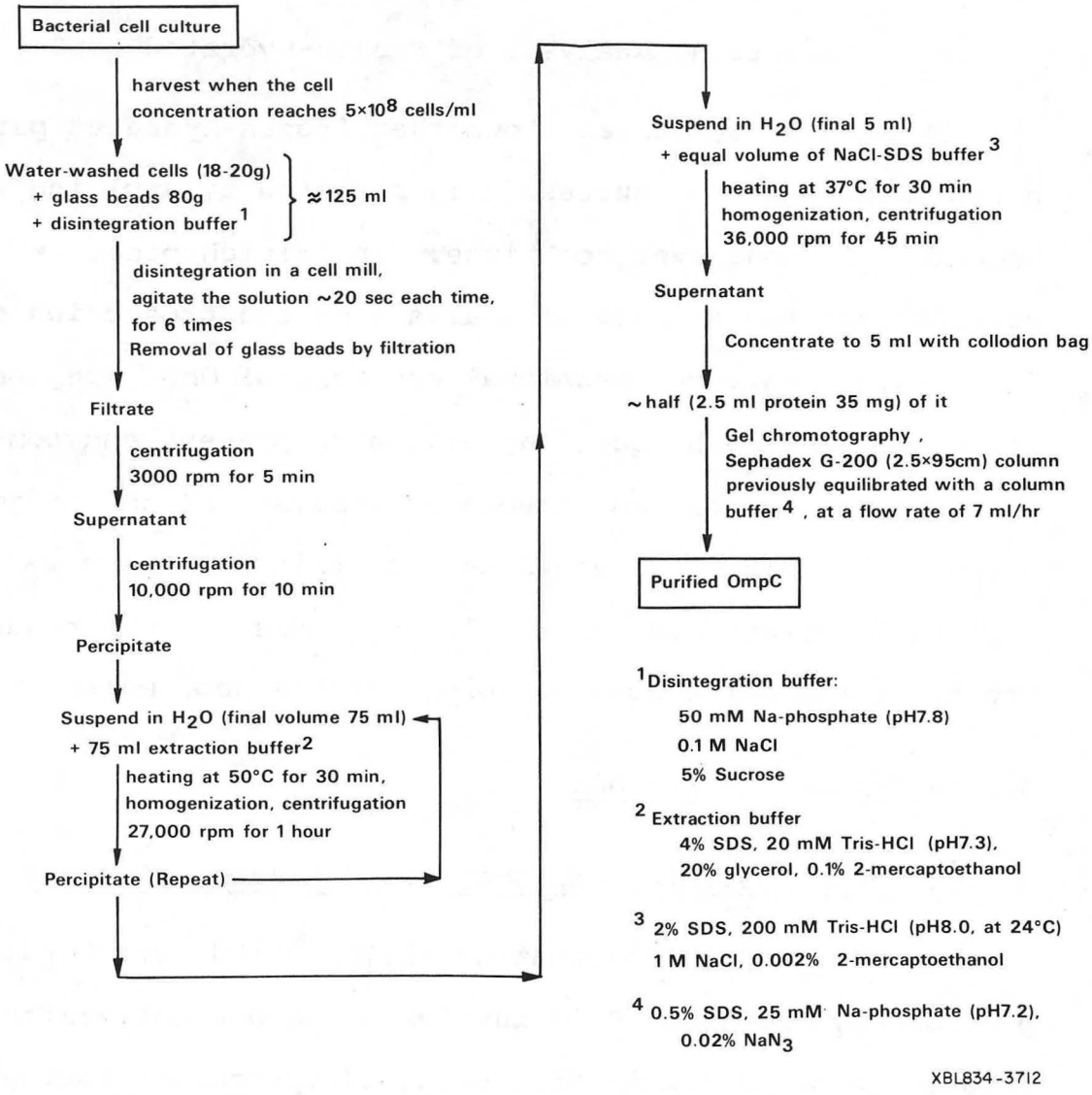

Fig. 4.1 Schematic diagram depicting the procedure of OmpC isolation and purification.

the Mizushima group, Yamada et al. (1978) reconstituted the purified OmpC with lipid A which had been isolated from the T-4 resistant strain E. coli YA21-6. Four hundred µg of purified OmpC (M.W. ~ 36,500) was incubated for 30 min with 0.5 M NaCl in 100 µl of 100 mM Tris-HCl pH 8.0, 1% sodium dodecylsulfate (SDS) and 0.1% 2-mercaptoethanol at 37° C . The solution was then mixed with 60 µg of lipid A (M.W. ~ 1,500) in 100 µl of 1% SDS. The mixture was dialyzed against 5 mM $MgCl_2$, 10 mM Tris-HCl pH 8.0, 0.025% 2-mercaptoethanol at 25° C for 48 hrs. The resulting precipitate was collected by ultracentrifugation and stored in distilled water with 0.02% NaN_3. The molar ratio of lipid A to OmpC used in this reconstitution procedure was ~ 4. A schematic diagram depicting the procedure of the reconstitution is shown in Fig. 4.2.

4.1.2 Electron Microscopy

(A) Specimen Preparation

Since the OmpC specimens tended to aggregate in stacked sheets, the solution was mildly vortexed before we applied the specimen to the EM grid.

(a) Negative Staining

Specimen preparation of negatively stained OmpC specimen was the same as that routinely used. However, the staining reagent used was uranyl formate prepared in a

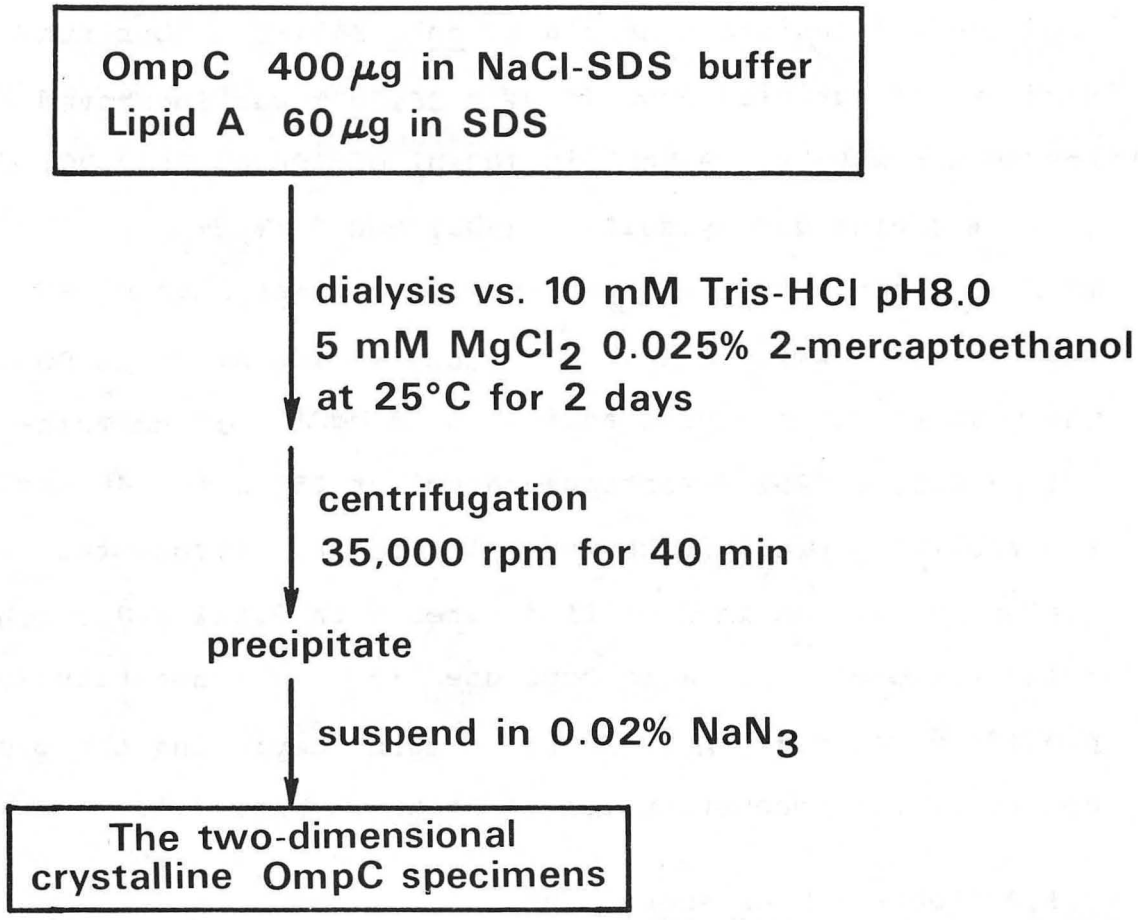

Fig. 4.2 Schematic diagram depicting the procedure of the reconstitution of OmpC specimen.

standard 1-cm cuvette and gave an absorbance value of 0.09 at a wavelength of 450 nm (Williams, 1981).

(b) Frozen Hydrated Specimens

The procedure for preparing frozen-hydrated OmpC was the same as that described in Chapter 3. However, after the specimen was deposited on the grid, another layer of polylysine was applied to the coverslip to ensure the adherence of the behenic acid monolayer to the surface of the coverslip. This modification of the frozen specimen preparation successfully expelled the bulk water. A low magnification image of OmpC specimens, Fig. 4.3, shows the distribution of the specimens on the grid.

(B) Image Recording

(a) Negatively Stained Specimens

The EM grid was scanned at an electron dose rate of at least 100 $e^-/Å^2$/min in order to ensure that good specimen areas were recorded. Images were recorded at a magnification of 40,000. The electron dose received by the specimen is at least 100 electron/$Å^2$.

(b) Frozen Hydrated Specimens

The procedures for scanning the EM grid and recording low dose micrographs were the same as those described in Chapter 3. Although it was easy to identify collapsed

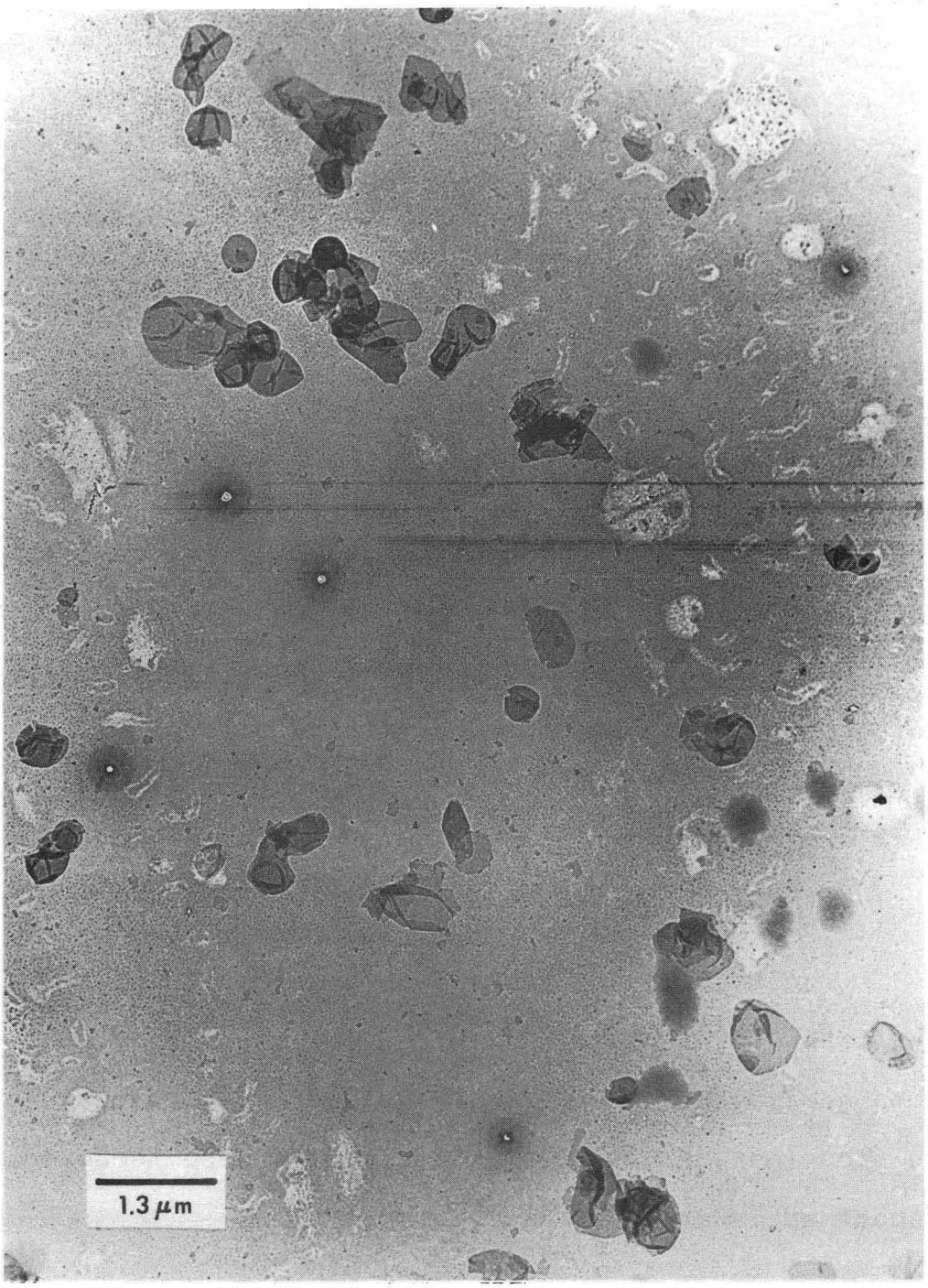

XBB 822-1176

Fig. 4.3 Low magnification image of an OmpC specimen which was prepared with the behenic acid monolayer technique. The image was recorded at room temperature and the specimen was air-dried.

vesicles while scanning the grid, it was sometimes difficult to locate single-layer membrane patches of OmpC. Therefore, we recorded micrographs at a magnification of 31,500 in order to cover more specimens per micrograph. The electron dose rate used to record the micrographs was ~ 5 electron/Å^2. The exposed Electron Image Films were developed in full strength D-19 developer for 12 min. The optical density of the films was ~ 1.1.

4.1.3. Computer Image Processing

Optical diffraction was again used to identify crystalline areas of the specimen on low dose micrographs. An area which produced high reflection orders in the optical diffraction pattern was digitized on a Perkin-Elmer PDS microdensitometer, using a data array 850-pixels long and 850-pixels wide. The sampling distance was 10 μm, which corresponded to ~3.2 Å at the specimen. All the subsequent data analyses were performed on a VAX 11/780 system at Lawrence Berkeley Laboratory, using computer programs which were written by Dr. D.A. Grano (1979).

In order to process the data from only the best part of the crystalline domain, the original 850 by 850 data array was divided into five 512 by 512 subarrays, shown in Fig. 4.4. These subarrays were Fourier transformed, and only the subarray in the center showed strong diffraction spots in the transform. We thus reduced the size of the

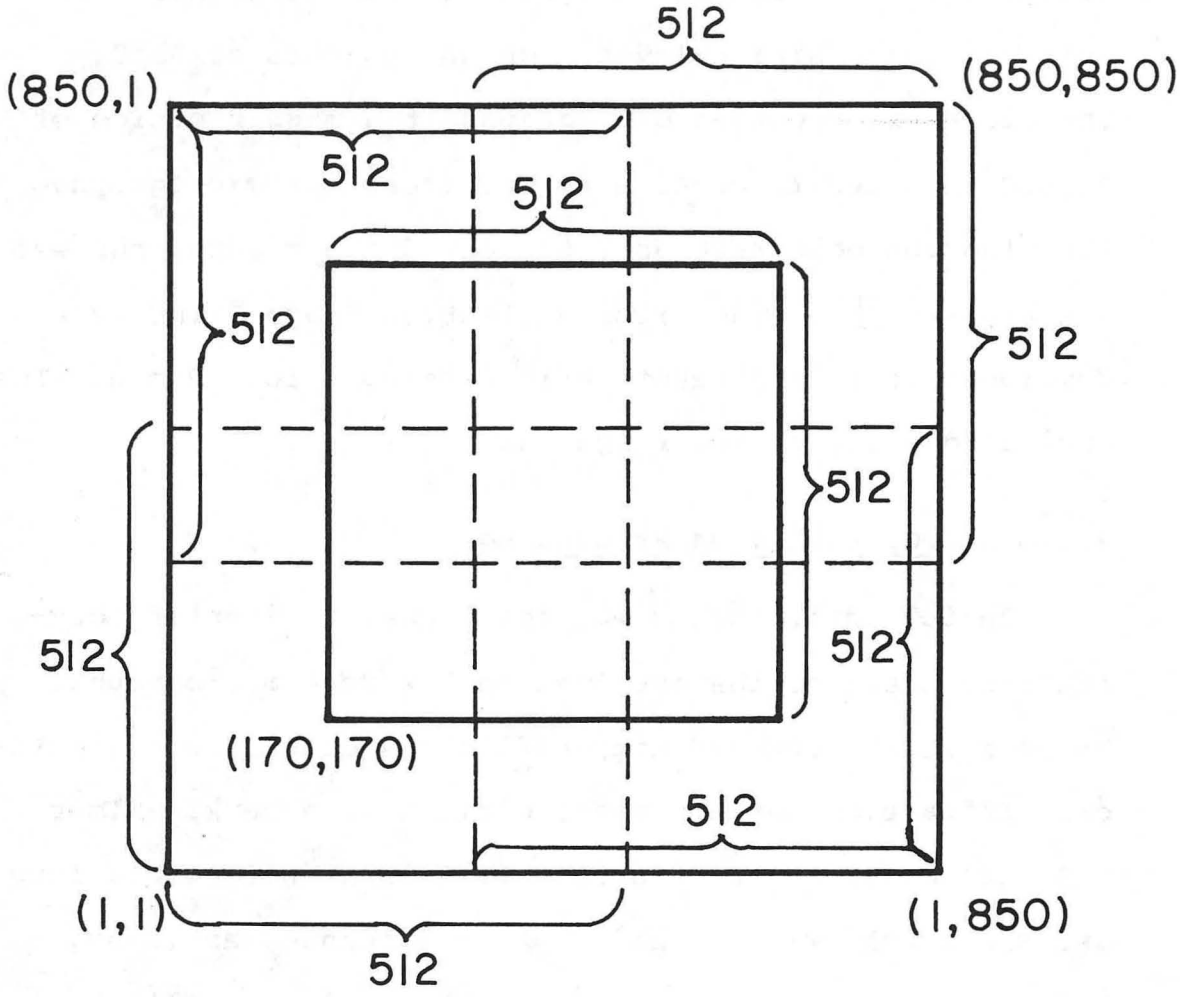

XBL836-3796

Fig. 4.4 Schematic diagram showing the division of the original 850 by 850 data array into five 512 by 512 subarrays.

raw data from a 850 by 850 data array to a 512 by 512 array.

In order to obtain a finer sampling of the Fourier map, we "floated" the data array, 512 by 512, into 1024 by 1024 data array. This floating process was performed by filling the empty surroundings with a value equal to the average of the values at the boundary of the original data array (DeRosier and Moore, 1970). The computed Fourier maps of these larger arrays showed a finer sampling in the row and the column directions.

The computed Fourier transform of the digitized data was first displayed with an overprint routine for a line printer. This overprint routine provided row and column numbers at the margin of the printout such that the location of strong reflections could be represented as points, (x,y), in the coordinate system. Strong reflections appeared as blurred spots in the overprint printout. We first estimated the position of the center-of-mass of each blurred spot. These positions, expressed as coordinates in rows and columns, were least-squares fitted by a "first round" reciprocal lattice.

When the "first round" reciprocal lattice was determined, the digital values of the amplitudes and the phases were displayed for each point in a 9 by 9 pixel array centered about every lattice point. However, the true

diffraction peak, or the highest value in each 9 by 9 array, might not be at the center of the array. This is because the position of strong reflections was not estimated accurately enough from the sample overprint display. The 9 by 9 digital display showed more precise locations of the strong reflections. Furthermore, from the amplitude variation around each high value in the array, we can estimate an even more precise location of the real peak, in a fraction of the numbers of rows and columns.

Using these refined locations, a reciprocal lattice was least-squares fitted again. This refinement of the reciprocal lattice was continued until the error between the manually identified positions of diffraction spots and the reciprocal lattice points generated by the least square fitting was less than two pixels for each strong reflection.

The phase values on the reciprocal lattice thus determined were further recalculated by searching for a phase origin, that is, one of the three-fold symmetry axes in a unit cell. In doing so, the phase error function, δP, representing the discrepancies between the phases of three-fold related reflections, was minimized. δP is defined as follows,

$$\delta P = \sqrt{\frac{\sum_{i=1}^{n}\sum_{j=1}^{3}\left(\bar{P}_i - P_{ij}\right)^2}{3n}}$$

where i is a number identifying a given triplet set,

j is the number identifying each member of a triplet,

n is the total number of triplet sets included in the phase origin refinement,

P_{ij} is the phase value of a reflection, calculated relative to the chosen origin.

$\overline{P}_i$ = is the average value, modulo 360^o, of the P_{ij}'s of a triplet.

In order to show how values of $\overline{P}_i$ are determined, we describe the algorithm that the computer software used to calculate $\overline{P}_i$. (a) P_{ij}'s are reordered such that $P_{i1} < P_{i2} < P_{i3}$. (b) If P_{i2} is greater than P_{i1} by more than 180^o, then 360^o is added to P_{i1}. If P_{i3} is greater than P_{i2} by more than 180^o, then 360^o is subtracted from P_{i3}. (c) These P_{ij}'s are then numerically averaged. In case that the average is greater than 360^o or less than o^o, we subtract or add 360^o respectively. The value thus obtained is the value of $\overline{P}_i$ used in the above equation.

We then averaged the amplitudes and averaged the recalculated phases, $\overline{P}_i$, of three-fold related reflections. These averaged coefficients were then incorporated into the restoration of computer-filtered images of the OmpC specimen. All the coefficients incorporated in the image restoration process were reversed in sign so that

positive values represent the high density regions of the specimen and negative values represent the low density regions.

The procedure of image processing of the negatively stained OmpC micrograph was almost the same as that used for the low dose image. However, the coefficients incorporated in the image restoration were not reversed in sign so that positive values represent the protein regions and negative values represent the stain-occupied regions.

4.2. Results

An image of OmpC specimens negatively stained with uranyl formate is shown in Fig. 4.5. The optical diffraction pattern of the image shows that the specimen exists in 2-dimensional hexagonal arrays with the highest reflection orders going out only to the (2,1). The coefficients incorporated in the image restoration are triplets of (1,0), (1,1), (2,1) and (1,2). The root-mean-square (RMS) phase error, associated with the function δP mentioned in the last section, is $\sim 12.85^{o}$. The computer filtered image of negatively stained OmpC, see Fig. 4.6, shows the geometric packing of the trimeric OmpC in the plane group p3. This filtered image is very similar to that of OmpC negatively stained with ammonium molybdate (Grano et al., 1982) and to that of OmpF negatively stained with phosphotungstate (Dorset et al., 1981).

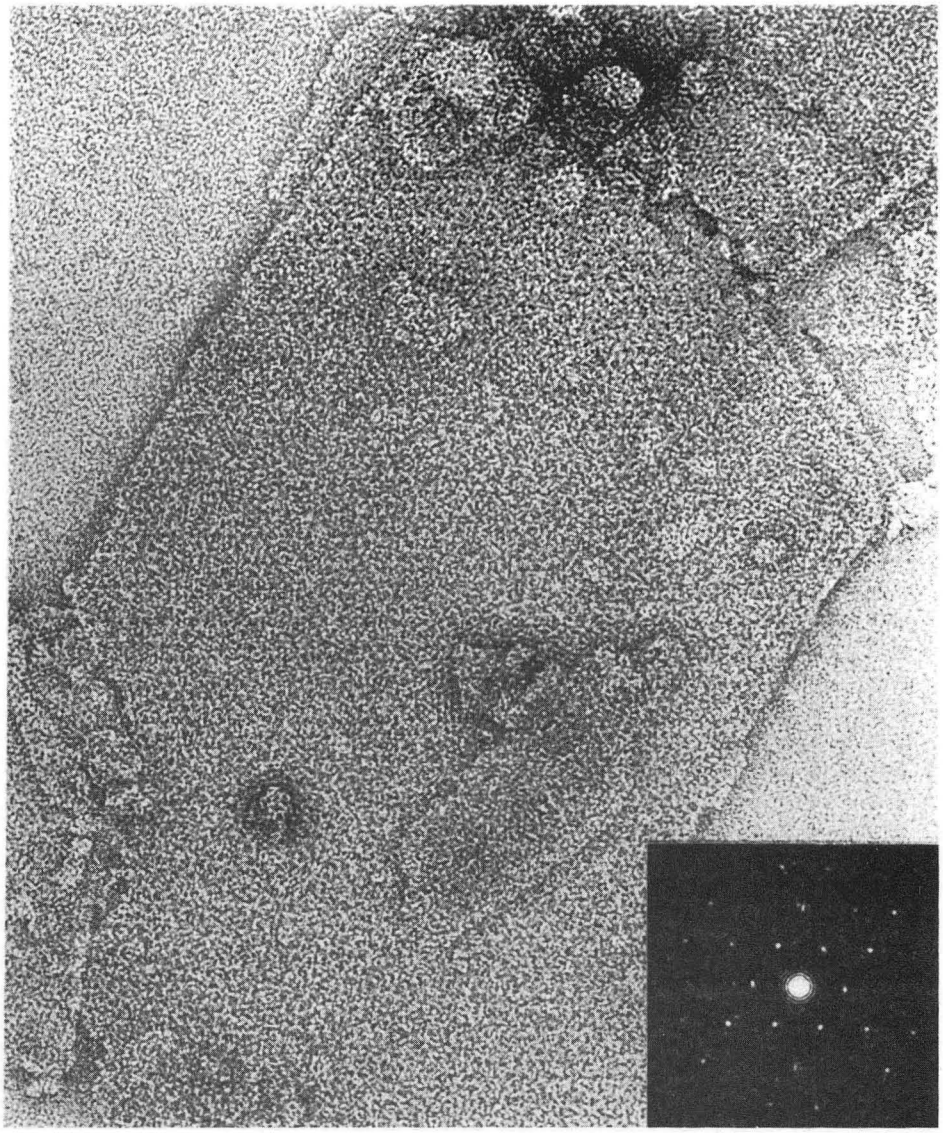

XBB 836-5334

Fig. 4.5 Image of OmpC specimens negatively stained with uranyl formate. The optical diffraction pattern of this image is shown at the lower left corner. The highest reflection order visible is the (2,1).

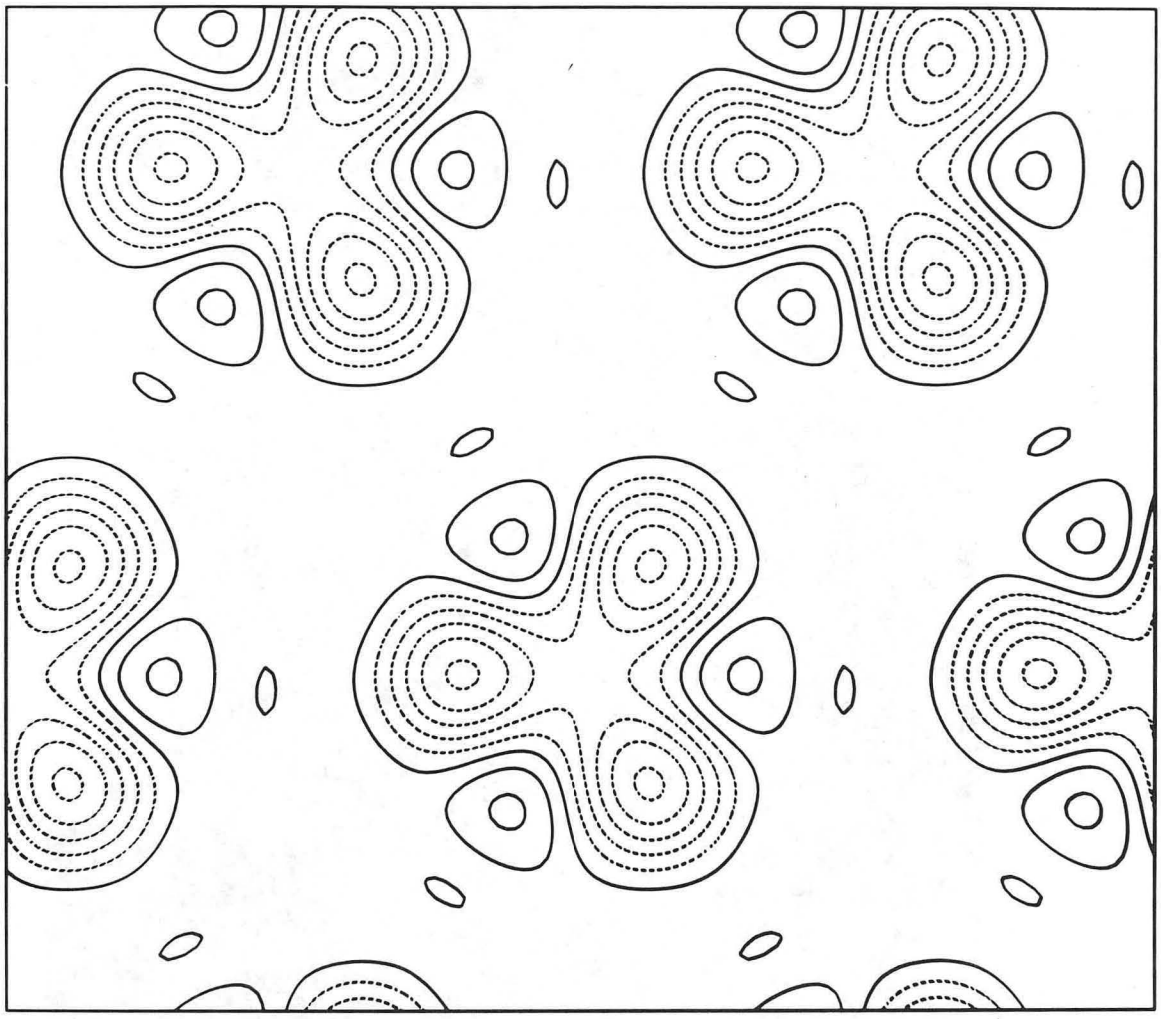

XBL 836-10286

Fig. 4.6 Computer filtered image of negatively stained OmpC showing the geometric packing of trimeric OmpC in the plane group p3. Positive contours represent the protein regions and negative contours represent stain-occupied regions.

A low dose image of frozen-hydrated OmpC specimens and an optical diffraction pattern of the image are shown in Fig. 4.7. The most pronounced features in the image are condensed ice crystals on the specimen. The OmpC membrane patches are essentially imperceptible. However, the optical diffraction pattern of the circled area shows strong intensities at a resolution of ~ 25 Å. The diffraction pattern shows a cluster of spots around the reciprocal lattice points. This fact indicates that this circled area is composed of several small crystalline domains each having a slightly different orientation. Meanwhile, analysis of the original 850 by 850 array, as mentioned in the previous section, also indicates that the size of coherent crystalline domains is very small (less than 0.15 μm on edge).

A portion of the computer output of the Fourier transform of the low dose image of frozen-hydrated OmpC specimen is shown in Fig. 4.8. This figure represents the amplitudes and the phases of the symmetry related triplet (2,0), (-2,2) and (0,-2). The circled numbers in each "amplitude array-box" are the digital representation of the reflection orders seen in the optical diffraction pattern, which is shown in Fig. 4.7. The phase values associated with the circled amplitudes were the values obtained before being recalculated relative to a three-

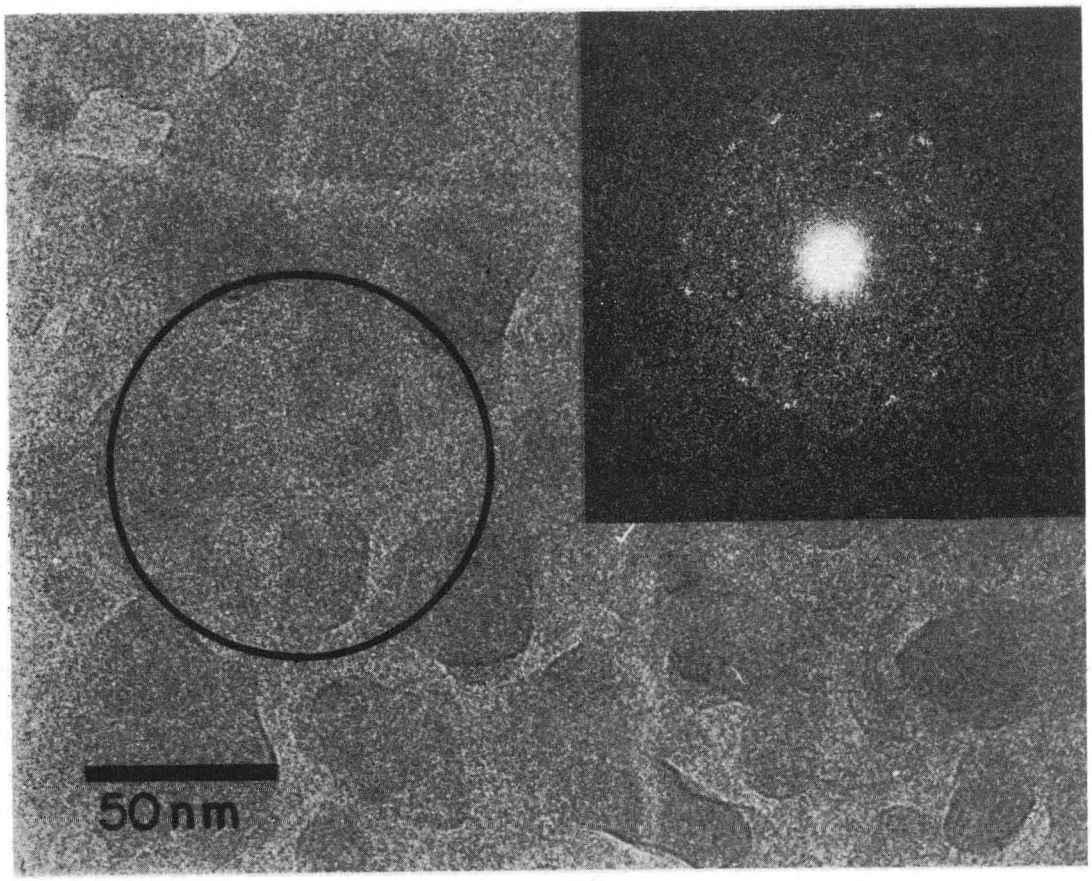

XBB 833-2080

Fig. 4.7 Low dose image of a frozen-hydrated OmpC specimen and its optical diffraction pattern. The OmpC membrane patches are essentially imperceptible. The optical diffraction pattern shows strong intensities at a resolution of ~ 25.4 Å.

Fig. 4.8 Computer output of the portion of the Fourier transform representing the amplitudes and phases of the symmetry related triplet (2,0), (-2,2) and (2,0). The low value of the amplitude of the (0,-2) must arise from the effect of noise which has not only a large amplitude but also a phase value which is ~ 180^{o} out of phase with the signal. The phase values associated with each reflection are the values before the process of the phase origin refinement.

H = 2 K = 0
LOCATION OF LARGEST PEAK IN BLOCK = (536, 611)
AMPLITUDE = 0.6968E+05 PHASE = 69.39
SCALE = 0.1E-01 MIDDLE = (536, 612)

AMPLITUDES

R C	608	609	610	611	612	613	614	615	616
532	226	118	204	169	212	74	191	246	293
533	322	351	153	138	100	210	46	212	273
534	255	316	122	359	225	194	267	136	316
535	111	176	179	626	535	152	347	13	291
536	86	177	225	697	642	276	260	201	151
537	215	223	145	456	428	334	132	172	125
538	197	118	48	60	63	288	311	156	168
539	338	153	180	287	254	214	465	293	66
540	420	178	268	306	170	177	360	194	263

PHASES

R C	608	609	610	611	612	613	614	615	616
532	248	292	360	322	258	249	30	355	301
533	236	259	317	12	264	233	168	41	359
534	210	255	337	53	61	232	225	96	58
535	184	245	40	65	80	186	243	281	88
536	288	242	50	69	93	156	259	330	96
537	295	260	27	66	105	162	225	357	71
538	333	300	299	10	178	179	167	121	66
539	33	60	202	251	269	183	158	155	9
540	55	94	199	238	260	152	153	191	283

H = -2 K = 2
LOCATION OF LARGEST PEAK IN BLOCK = (417, 485)
AMPLITUDE = 0.7128E+05 PHASE = 134.22
SCALE = 0.1E-01 MIDDLE = (417, 485)

AMPLITUDES

R C	481	482	483	484	485	486	487	488	489
413	307	359	103	179	169	134	116	127	173
414	223	283	277	157	90	245	323	287	273
415	103	144	250	284	273	308	290	149	94
416	147	138	47	228	495	424	72	191	113
417	318	449	370	487	713	409	215	373	97
418	352	474	519	430	608	342	172	296	15
419	128	203	352	276	225	306	162	164	80
420	170	495	458	217	318	481	267	161	195
421	313	501	448	278	203	451	383	136	297

PHASES

R C	481	482	483	484	485	486	487	488	489
413	356	338	312	164	139	86	104	182	237
414	2	311	286	250	146	101	112	151	202
415	355	275	269	249	203	154	127	130	185
416	341	346	344	174	168	165	206	326	35
417	355	3	40	111	134	147	290	312	37
418	331	13	43	89	121	141	282	306	12
419	321	87	79	86	155	192	233	323	1
420	170	159	143	148	223	232	247	350	39
421	172	177	157	142	223	254	270	340	71

H = 0 K = -2
LOCATION OF LARGEST PEAK IN BLOCK = (589, 447)
AMPLITUDE = 0.4372E+05 PHASE = 112.93
SCALE = 0.1E-01 MIDDLE = (586, 443)

AMPLITUDES

R C439	440	441	442	443	444	445	446	447
582	129	182	265	133	75	84	86	170	187
583	104	50	149	276	316	281	115	69	41
584	220	304	69	178	204	242	196	118	150
585	164	298	234	201	258	266	265	151	56
586	108	135	232	280	395	406	352	235	152
587	270	97	89	122	125	193	122	59	110
588	242	84	69	162	213	128	197	406	196
589	231	208	175	21	238	182	154	387	437
590	180	225	212	125	286	332	119	126	374

PHASES

R C439	440	441	442	443	444	445	446	447
582	285	27	58	83	192	221	263	261	230
583	215	142	43	39	59	79	79	309	276
584	204	186	215	6	52	101	112	76	51
585	238	177	185	236	240	208	182	170	39
586	2	126	161	208	234	228	206	206	276
587	73	77	128	139	190	214	191	89	298
588	114	205	315	77	118	141	56	57	95
589	160	235	289	179	170	184	38	60	113
590	264	279	306	272	211	212	241	53	107

fold symmetry origin.

From the least-square fitting procedures, we obtained a reciprocal lattice with unit vectors $a^* = 0.99\ b^*$, and the angle between them, γ^*, was 59.11°. The RMS phase error of the coefficients incorporated in the image restoration was ~ 23.3°. The highest reflection order incorporated in the phase origin refinement procedure corresponds to a resolution of ~ 13.5 Å.

The signal-to-noise ratio of the diffraction peaks was evaluated by comparing the amplitude of each reflection to the mean and the standard deviation of the 9 by 9 pixel arrays containing the reflection. The results of these calculations for the reflection orders that were included in the restoration are shown in Table 4.1.

Fig.'s 4.9-4.12 show contour plots of computer filtered images synthesized from various sets of triplet coefficients. Fig's. 4.9-4.12 were synthesized from the triplets which are at least 1.5, 2.0, 2.4, 3.0 standard deviation above the mean, respectively. As long as one reflection in a triplet has a peak amplitude that is the specified number of standard deviations above the mean, the amplitudes and the phases of the triplet were averaged and then incorporated into the Fourier synthesis. Positive contours, shown as solid lines, represent protein domains. Negative contours, shown as fainter, dotted lines,

Table 4.1 Calculations of the signal-to-noise ratio for reflection orders used in the structural analysis of frozen-hydrated OmpC. Phase values for each reflection are relative to a crystallographic three-fold axis.

H	K	Phase	Amplitude	Mean	Standard Deviation (σ)	(Amplitude-Mean)/σ
1	1	78.4	62500	23290	10780	3.64
-2	1	81.5	69100	21620	12510	3.80
1	-2	56.1	74530	24250	11530	4.36
2	0	219.6	69700	20920	9590	5.09
-2	2	285.6	71300	23060	11460	4.21
0	-2	285.8	40600	20190	10150	2.00
1	2	114.5	78900	22680	10630	5.29
-3	1	134.2	70100	25680	15030	3.08
2	-3	161.3	46300	19830	10650	2.49
2	1	106.7	63500	21110	10790	3.93
-3	2	67.3	42700	24170	13140	1.41
1	-3	107.0	35700	15520	8680	2.32
2	2	164.8	15500	12910	7790	0.33
-4	2	119.0	30000	13420	7260	2.28
2	-4	211.2	42300	16390	11060	2.34
1	3	195.6	29500	15930	7150	1.90
-4	1	238.9	28600	15550	8820	1.48
3	-4	191.5	21200	18500	8900	0.30
4	0	351.2	30800	16550	8770	1 62
-4	4	31.2	31300	16050	7400	2.06
0	-4	339.6	39100	15890	6830	3.40
3	2	268.1	25100	14640	7060	1.48
-5	3	216.8	33800	14530	7830	2.46
2	-5	240.1	20300	13640	7050	0.94
5	0	340.5	26600	13840	7590	1.68
-5	5	5.0	33600	15400	8410	2.16
0	-5	329.5	24500	13000	6520	1.76

XBL 836-10202

represent regions that contain substantial amount of lipids and/or water. In the lower portion of each figure, the solid dots of a hexagonal array represent the coefficients that were incorporated in the image restoration of OmpC. Each contour plot covers a slightly different range of intensity values; however, all four plots are displayed with the same contour interval value.

4.3. Discussion

The existence of condensed ice crystals caused several problems: (a) The optical diffraction patterns of low dose images did not show the contrast transfer function, $\sin\{\gamma(S)\}$, where

$$\gamma(S) = \frac{2\pi}{\lambda}\left(\frac{C_s\lambda^4 S^4}{4} - \frac{\Delta z \lambda^2 S^2}{2}\right),$$

where C_s = the spherical aberration coefficient of the objective lens, Δ Z = the defocus value of the lens. It was thus impossible to assess the specimen drift and the lens astigmatism. (b) We had to start recording micrographs within ≈ 30 min after the specimen had been transferred into the stage. Otherwise, the condensed ice became so thick that we could not identify the OmpC membrane patches. However, thirty minutes often appeared to be insufficient to allow the specimen cartridge and the stage to reach thermal equilibrium. Therefore, a specimen drift often occurred.

Fig. 4.9 Contour plot of a computer filtered image of frozen-hydrated OmpC specimen. Coefficients used in the image restoration are shown in the lower half of the figure. The first positive contour represents a value of 3.0. The maximum value in this contour plot is 11.0 and the minimum is -21.0. The highest reflection incorporated in this image restoration corresponds to a resolution of ~ 13.5 Å.

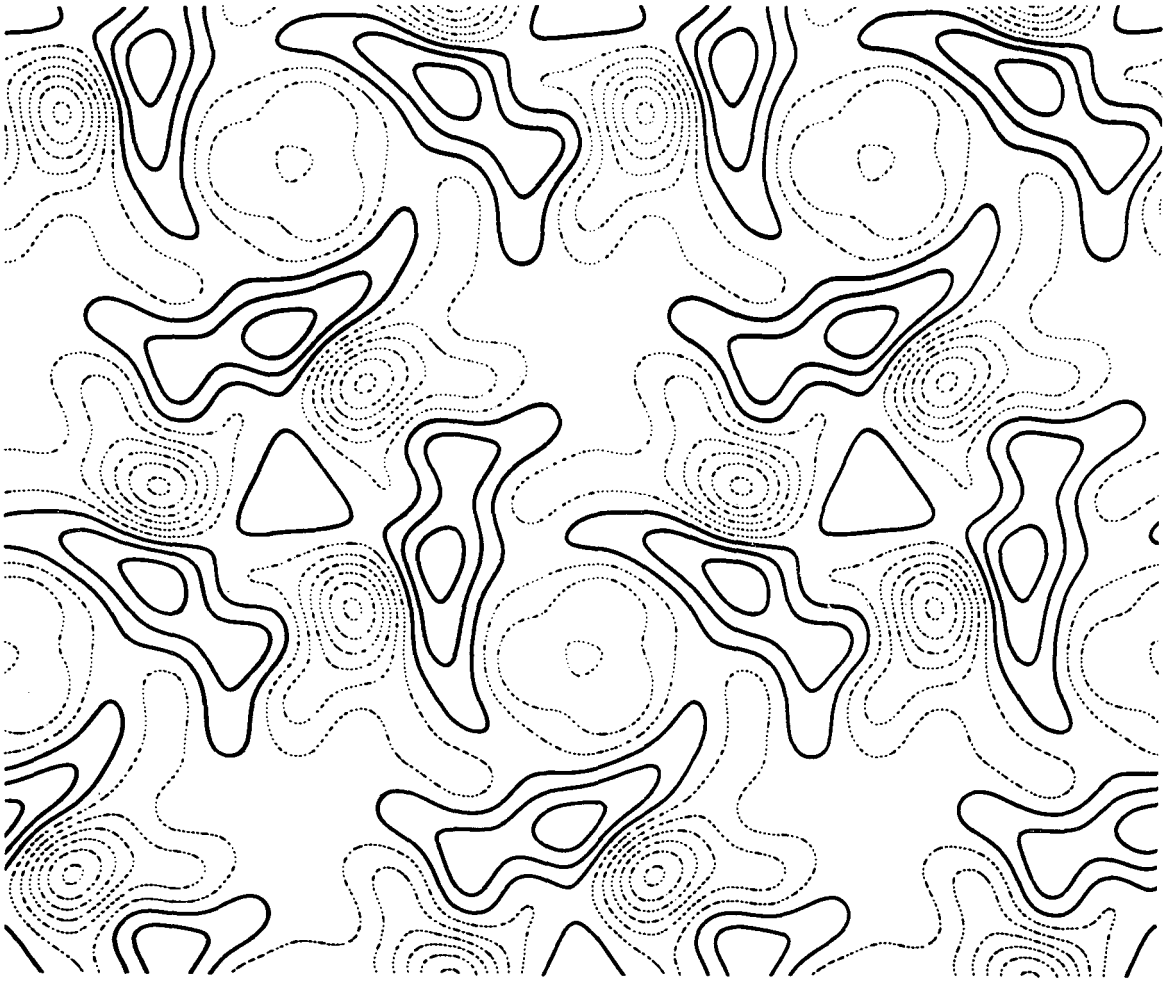

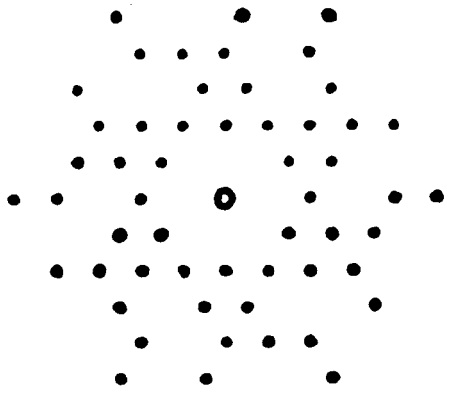

XBB 836-5022

Fig. 4.10 Contour plot of a computer filtered image of a frozen-hydrated OmpC specimen. Coefficients used in the image restoration are shown in the lower half of the figure; the (1,3), (-4,1) and (3,-4) triplet of reflections are the only Fourier coefficients that were used in generating Fig. 4.9, which are not included in this filtered image. The first positive contour represents a value of 2.0. The maximum value in this contour plot is 10.0 and the minimum is -22.0. The highest reflection incorporated in this image restoration again corresponds to a resolution of ~ 13.5 Å.

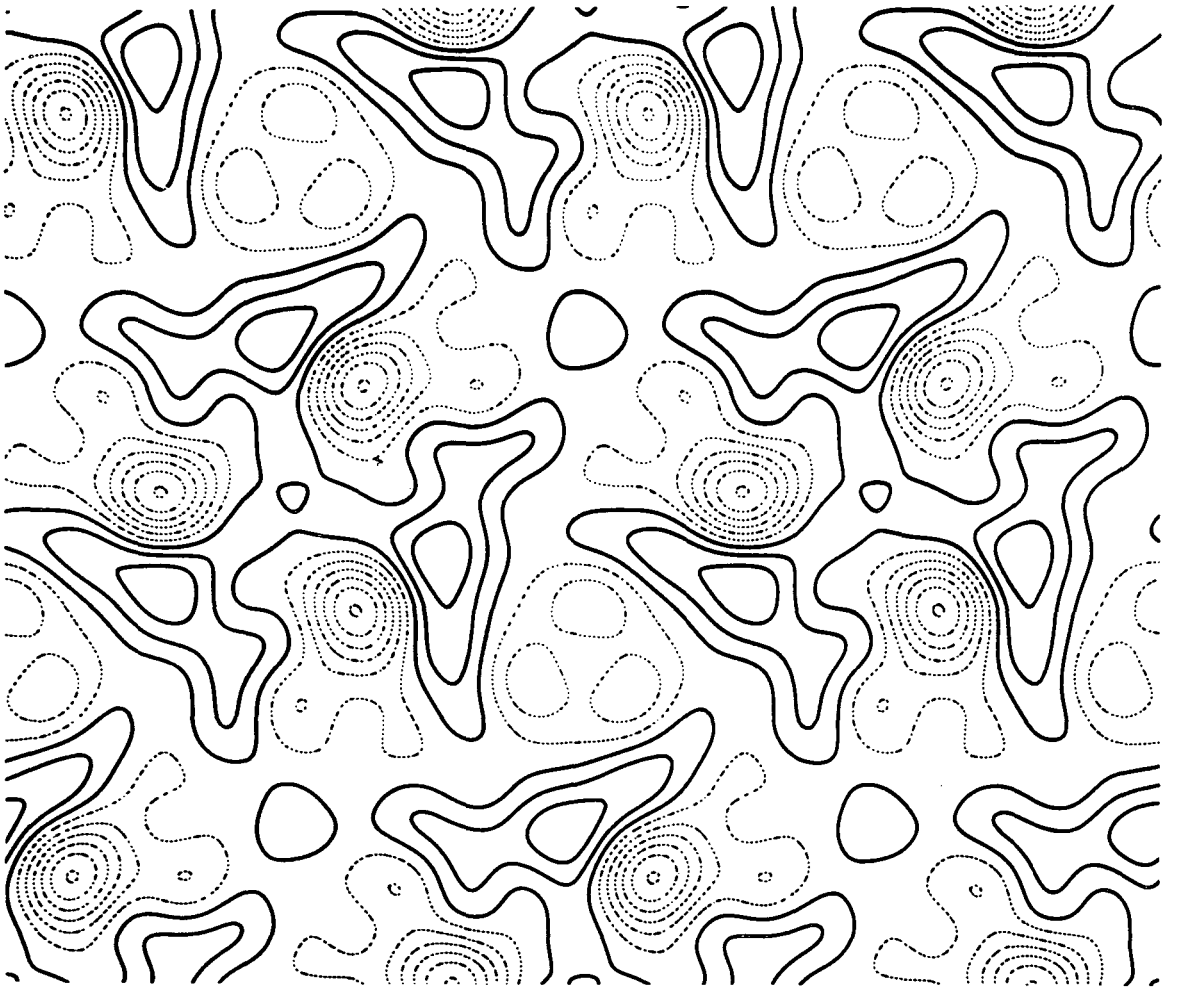

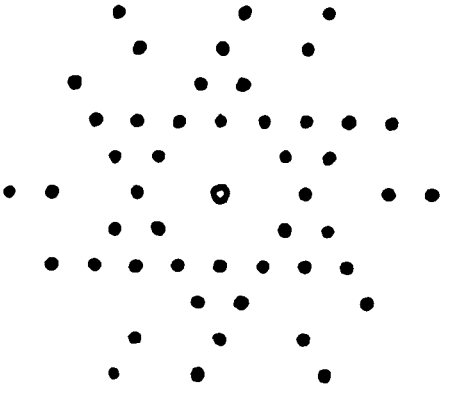

XBB 836-5021

Fig. 4.11 Contour plot of a computer filtered image of a frozen-hydrated OmpC specimen. Coefficients used in the image restoration are shown in the lower half of the figure. The first positive contour represents a value of 0.8. The maximum value in this contour plot is 8.8 and minimum is -19.2. The highest reflection incorporated in this image restoration corresponds to a resolution of ~ 15.5 Å.

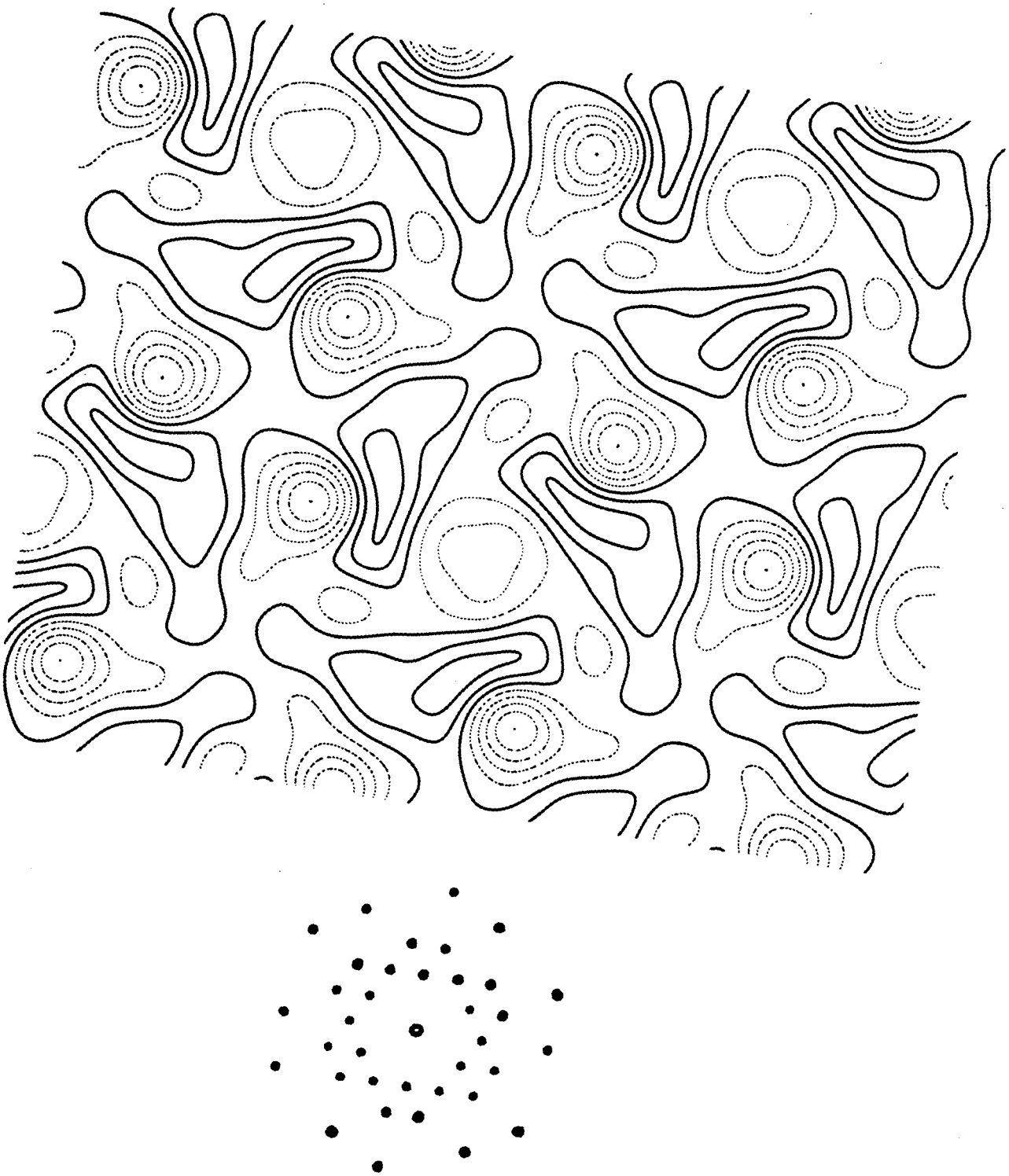

XBB 836-5024

Fig. 4.12 Contour plot of a computer filtered image of a frozen-hydrated OmpC specimen. Coefficients used in the image restoration are shown in the lower half of the figure. The first positive contour plot is 10.1 and the minimum is -17.9. The highest reflection incorporated in this image restoration corresponds to a resolution of ~ 16.8 Å.

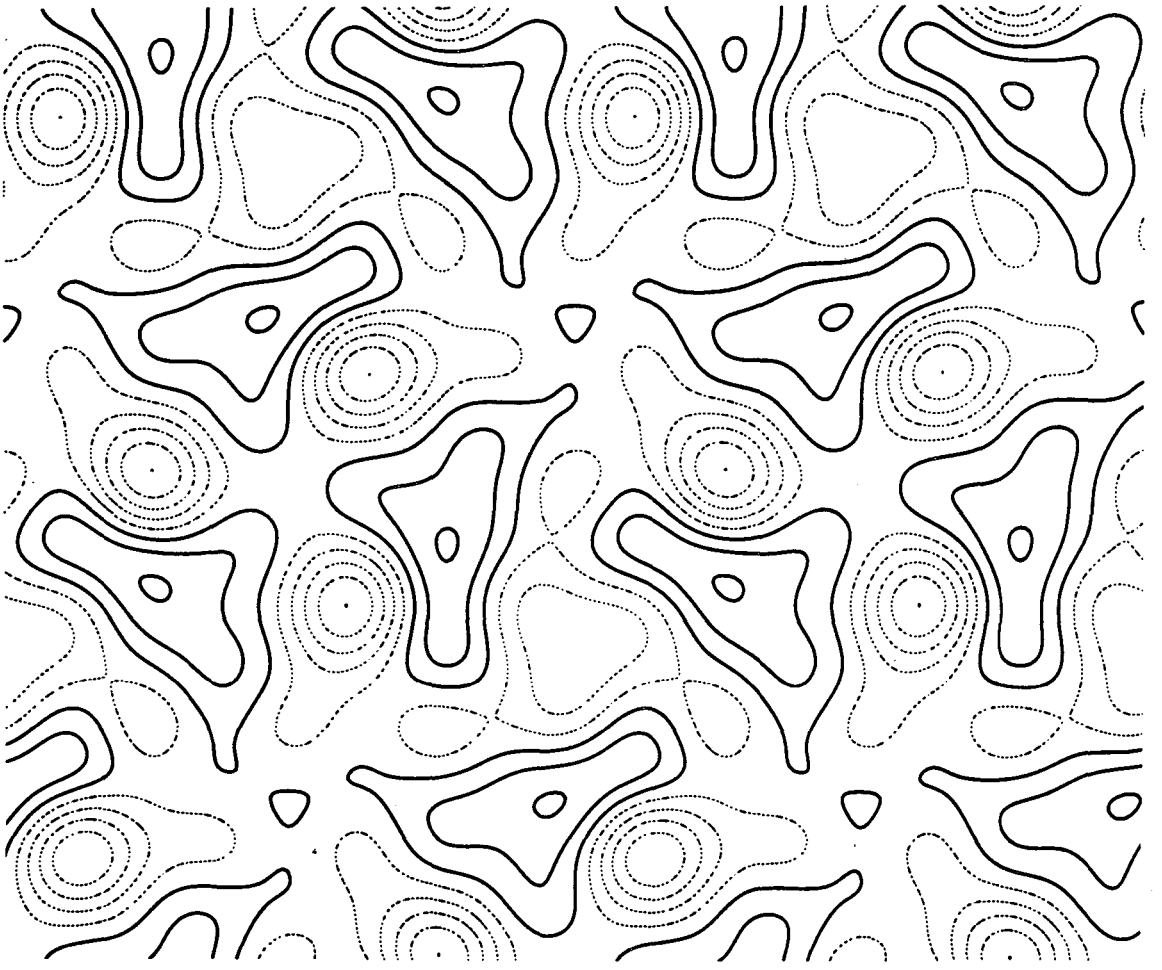

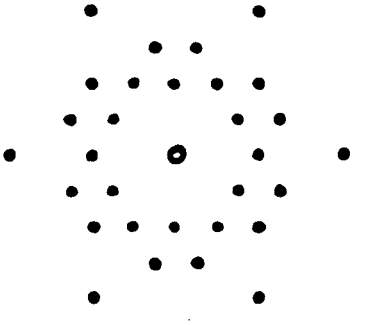

XBB 836-5023

Despite these problems, we were able to obtain low dose images of frozen-hydrated OmpC specimens at moderate resolution. The optical transform of the image shown in Fig. 4.7, shows no systematic azimuthal variation of diffraction intensities. Even though we could not observe the contrast transfer function, we conclude that specimen drift and astigmatism do not affect the image out to the resolution of the visible (detectable) diffraction spots.

In Fig. 4.8, the three-fold symmetry related triplet does not have a similar amplitude at all three lattice points. The amplitude of the (0,-2) is only 0.57 of the value at the other two lattice points. Since there is no specimen drift and astigmatism that is evident in the optical transform at this resolution, this discrepancy must arise from the fact that the noise amplitude on the (0,-2) reflection is fairly large and the noise phase is ~ 180^{o} out of the phase of the signal.

Partial specific volumes of phospholipids in general are ~ 1.1 ml/g (Tanford et al., 1974). The ratio of the number of phosphate groups to the number of fatty acid chains in lipid A is very similar to that in phospholipid. Therefore, the mass density of lipid A is estimated to be ~ 0.9 g/ml which is smaller than that of H_2O, 1.0 g/ml, and a lot smaller than that of protein, 1.3 g/ml. Based on these data, we naturally interpret the positive con-

tours to represent the regions of protein and the area with several negative contour levels to represent the regions of a lipid bilayer. The area with less negative contour levels are speculated to be the water channels.

The assignment of the water channels is consistent with the result of the 3-D structural studies of negatively stained OmpF at a resolution ~ 20 Å (Engel et al., unpublished data). In this study, it was shown that three water channels merge together as they span across the membrane. The projection in the region of the water channels is therefore composed of a fraction of protein. As a result, the averaged density is less negative than that of the lipid bilayer. Fig. 4.13, a duplicate of Fig. 4.9, shows the assignment of regions of protein, lipid A and water channels.

In Fig.4.13, each protein monomer has a narrow, elongated domain of high density. As we have mentioned in Chapter 1, OmpC has a high content of β-structure. We therefore interpret this narrow, elongated domain as a projection of a layer of β-sheet which spans the lipid bilayer perpendicularly.

Furthermore, the shape of the protein domain in the frozen-hydrated specimen is quite different from the near-circular one shown in the filtered image of negatively stained OmpC, Fig. 4.6. This difference must arise

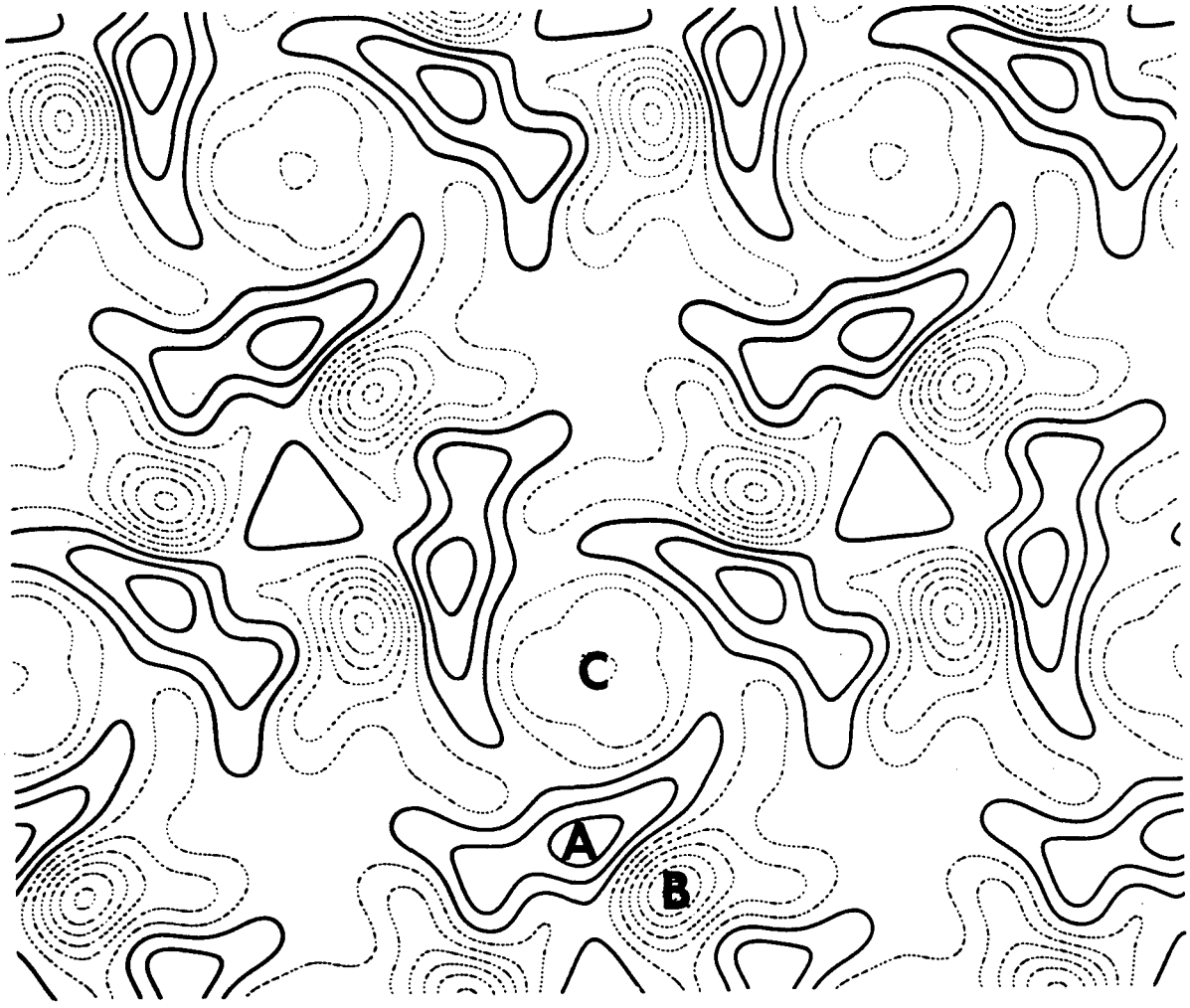

XBB 836-5022A

Fig. 4.13 Assignment of regions of protein, lipid A and water channels. Protein is labeled with A, lipid A is labeled with B and water channels are labeled with C.

from the fact that the negatively stained image only shows the topography of aqueous spaces and cannot provide information about the internal structure of the protein. On the other hand, the contrast in the frozen hydrated specimen reflects the fact that the density of the protein domain is much larger than that of ice and lipids. In the image of frozen-hydrated specimens, therefore, the protein domain can be easily identified.

Comparing the information obtained from the image of frozen-hydrated specimens and that of negatively stained specimens, we found that the high contour level in the frozen image and the high contour level in the negatively stained image represent the portion of the protein monomer which spans the bilayer and protrudes into the aqueous environment. From a single projection, we will not be able to tell on which side of the membrane the "excess" protein is located. However, it may be possible to answer this question by freeze-drying and shadowing the specimen.

We also found that the geometric packing of OmpC in these two cases is slightly different. With respect to the three-fold symmetry axis, there is a relative rotation, ~ 25°, between the protein domain in the negatively stained image and the high density domain in the frozen images. This rotation may be due to no more than the fact that the negatively stained image is unable to demonstrate

substantial handedness, or deviation from mirror symmetry.

One trivial reason which accounts for the presence of mirror symmetry of the protein trimer in the image of negatively stained OmpC is that the specimen appears to be a collapsed vesicle, see the image of Fig. 4.5. Two layers of the specimen are therefore superimposed on top of each other with opposite orientations. As a result, the projection of the collapsed vesicle should possess a mirror symmetry.

We have to be cautious when discussing the differences between these two images. The electron doses received by the specimen are quite different in these two cases. As we have mentioned in Chapter 2, the staining reagent will redistribute and migrate within a unit cell when the electron dose received by the specimen exceeds 100 electrons/$\AA^2$. Therefore, it is very possible that when we try to interpret certain features, such as the separation between the aqueous channels or the diameter of each channel, the image of negatively stained OmpC does not reflect the real structure.

There was no signal-to-noise evaluation on the coefficients used for image restoration of negatively stained OmpC. From the computer output of the 9 by 9 arrays, it was easy to observe numerically that the coefficients have a high signal-to-noise ratio. In addition, it is also

shown in the optical transform of Fig. 4.5 that the intensities of the triplets (1,0), (1,1), (1,2) and (2,1) are easily detectable. Therefore, it is not necessary to pursue the quantitative evaluation of these triplets.

In the image restoration of frozen-hydrated OmpC, we incorporated coefficients corresponding to a resolution of 13.5 Å. Coefficients with a higher reflection order than the (2,1) were not visible in the optical diffraction pattern. In order to evaluate how trustworthy these coefficients are, we compared the amplitude of each reflection to the mean of the 9 by 9 array. In Table 4.1, for each triplet, there is at least one reflection which is 1.9 standard deviations above the mean. The figure of merit (Hayward and Stroud, 1981) of the reflection with this value, 1.9, is ~ 0.82 (Downing, personal communication). The fact that the reflections were on the lattice, with a RMS phase error 23.2° and the figure-of-merit is ≈ 0.82 makes us feel confident about the data used for the image restoration.

As shown in Table 4.1, the Fourier coefficients at higher resolution, beyond the (5,0) reflection orders, have a small signal-to-noise ratio. Further work on analyzing data from a large number of small regions, each containing a single coherent crystalline domain, could result in the retrieval of high-resolution data sets with

a better signal-to-noise ratio. After a common phase origin is identified, Fourier coefficients from these small crystalline domains can be superimposed. High-resolution signals will build up a lot faster than noise. Furthermore, by combining these data from each coherent crystalline domain, we will also improve the signal-to-noise ratio of the lower resolution coefficients which were not incorporated in the image restoration. This approach has been successfully applied to determine the projected structure of the purple membrane at a resolution of 3.7 Å by low temperature electron microscopy (Hayward and Stroud, 1981).

CHAPTER 5

Summary and Conclusions

A method of preparing frozen-hydrated specimens for low temperature electron microscopy has been developed. The method, referred to here as the behenic acid monolayer technique, has been shown to successfully preserve specimens in a frozen-hydrated state. Electron diffraction patterns and low dose images of bacteriorhodopsin have been recorded and the structural information obtained from these studies are ~ 7 Å and 10 Å respectively.

The behenic acid monolayer technique has been applied to the structure analysis of OmpC by high-resolution electron microscopy. Low dose images of OmpC specimens have been obtained. The optical diffraction pattern of a low dose image shows strong intensities at the (2,1) reflection order. Computer processing of the image has been performed, and a computer filtered image of the specimen containing structural information of OmpC at a resolution of ~ 13.5 Å has been produced.

The filtered image of negatively stained OmpC has also been presented. The negatively stained specimen shows only the topography of aqueous spaces and cannot provide information about the internal structure of the protein. In the frozen-hydrated OmpC image, the protein domain can be easily identified. This study shows that in

the frozen-hydrated case, each protein monomer has a narrow, elongated domain of high density. In the case of the negatively stained sample, the protein domain is shown as a small, near-circular domain.

Comparing results of the structural analysis of the projection of frozen-hydrated OmpC and negatively stained OmpC, we can identify a domain of the OmpC monomer which protrudes beyond the membrane bilayer, into the aqueous environment. However, it is not possible to determine on which side of the membrane this protruding mass is located. One quick and simple method that may provide this extra information is to look at specimens which have been freeze-dried and shadowed.

Combining the results from the 3-D structural studies of negatively stained specimens, we identified the regions of protein, lipid A and the water channels. Furthermore, from the results obtained from spectroscopic studies of the secondary structures of the peptide chain, we interpret the protein region in the image of the frozen-hydrated OmpC to represent the projection of a layer of β-sheet which spans the lipid bilayer perpendicularly.

In order to increase the signal-to-noise ratio of the coefficients which were not incorporated in the image restoration of frozen-hydrated OmpC, a method has been proposed which involves combining Fourier coefficients from

many small but highly coherent crystalline domains. A similar technique has been successfully applied to determine the projected structure of the purple membrane at a resolution of 3.7 Å (Hayward and Stroud, 1981). In doing so, we should expect the structural information of frozen-hydrated OmpC will be obtained at a higher resolution than what we have obtained in this study, 13.5 Å.

Once the specimen preparation techniques of low temperature electron microscopy have been developed, the structural analysis of membrane proteins by electron microscopy certainly should proceed very fast. Many two-dimensional crystals of membrane proteins have been obtained by the reconstitution of membrane proteins with phospholipids. Furthermore, membrane proteins have been difficult to grow as three-dimensional crystals which are big enough for X-ray crystallography study. It is, therefore, likely that low dose, low temperature electron microscopy will be the unique technique for the structural determination of membrane proteins.

REFERENCES

1. Anderson, T.F. (1954) "Some Fundamental Limitations to the Preparation of Three-Dimensional Specimens for the Electron Microscope," Trans. N.Y. Acad. Sci. 16, 242-249.

2. Anderson, T.F. (1956) "Preservation of Structure in Dried Specimens," Proceedings III Int. Conf. Electron Micro., Lodon 122-129.

3. Braun, V. and K. Rehn (1969) "Chemical Characterization, Spatial Distribution and Function of a Lipoprotein (Murein-Lipoprotein) of the E. coli Cell Wall: The Specific Effect of Trypsin on the Membrane Structure," Eur. J. Biochem. 10, 426-438.

4. Blodgett, K.B. (1935) "Film Built by Depositing Successive Monomolecular Layers on a Solid Surface," J. Am. Chem. Soc. 57, 1007-1022.

5. Boyde, A. and C. Wood (1969) "Preparation of Animal Tissues for Surface-Scanning Electron Microscopy," J. Micro. 90, 221-249.

6. Chen, R.,C. Kramer, W Schmidmayr and U. Henning (1979) "Primary Structure of Major Outer Membrane Protein I of Escherichia coli B/r," Proc. Natl. Acad. Sci. 76, 5014-5017.

7. Cosslett, V.E. (1978) "Radiation Damage in the High Resolution Electron Microscopy of Biological Materials: A Review," J. Microscopy 113, 113-129.

8. DeRosier, D.J. and P.B. Moore (1970) "Reconstruction of Three-dimensional Images from Electron Micrographs of Structures with Helical Symmetry," J. Mol. Biol. 52, 355-369.

9. DiRienzo, J.M., K. Nakamura and M. Inouye (1978) "The Outer Membrane Proteins of Gram-Negative Bacteria: Biosynthesis, Assembly, and Functions," Annu. Rev. Biochem. 47, 481-532.

10. Dorset, D.L.,A. Engel, R.M. Garavito and J.P. Rosenbusch (1981) "Crystal Packing of E. coli Porin (Matrix Protein)," Proc. Electron Micro. Soc. Am. 39, 42-43.

11. Fullam, E.F. (1972) "A Closed Wet Cell for the Electron Microscope," Rev. Sci. Instrum. 43, 245-247.

12. Garavito, R.M. and J.P. Rosenbusch (1980) "Three Dimensional Crystals of An Integral Membrane Protein: An Initial X-Ray Analysis," J. Cell Biol. 86, 327-329.

13. Garavito, R.M.,J.A. Jenkins, J.M. Neuhaus, A.P. Pugsley and J.P. Rosenbusch (1982) "Structural Investigations of Outer Membrane Proteins from Escherichia coli," Ann. Microbiol. (Inst. Pasteur) 133 A, 37-41.

14. Glaeser, R.M. (1971) "Limitations to Significant Information in Biological Electron Microscopy as a Result of Radiation Damage," J. Ultrastruc. Res. 36, 466-482.

15. Glaeser, R.M. (1975) "Radiation Damage and Biological

Electron Microscopy," Physical Aspects of Electron Microscopy and Microbeam Analysis, edited by B.M. Siegel and D.R. Beaman (John Wiley and Sons Inc., New York) 205-230.

16. Glaeser, R.M. and K.A. Taylor (1978) "Radiation Damage Relative to Transmission Electron Microscopy of Biological Specimens at Low Temperature: A Review, " J. Micro. 112, 127-138.
17. Glaeser, R.M. (1979) "Radiation Damage with Biological Specimens and Organic Materials," Introduction to Analytical Electron Microscopy, edited by J.J. Hren, J.I. Goldstein and D.C. Joy (Plenum Publishing Corporation, New York) 423-436.
18. Grano, D.A. (1979) "Three-Dimensional Reconstruction in Electron Microscopy," Ph.D. Thesis.
19. Grano, D.A.,C.F. Chang and R.M. Glaeser (1982) "Structural Investigations of the Pore-Forming OmpC Protein from E. coli," Proc. Electron Micro. Soc. Am. 40, 90-91.
20. Grubb, D.T. and A. Keller (1972) "Beam-Induced Radiation Damage in Polymers and Its Effects on the Image Formed in the Electron Microscope," Electron Microscopy (Institute of Physics, London) 554-560.
21. Harada, Y.,T. Taoka, M. Watanabe, M. Ohara, T. Kobayashi, and N. Uyeda (1972) "Effect of Accelerating Voltage and Specimen Temperature on Radiation Damage

of Hexadecachloro Copper Phthalocyanine," Proc.Electron Micro. Soc. Am. 30 686-687.

22. Hayward, S.B. and R.M. Glaeser (1979) "Radiation Damage of Purple Membrane at Low Temperature," Ultramicroscopy 4, 201-210.

23. Hayward S.B. and R.M. Glaeser(1980) "High Resolution Cold Stage for the JEOL 100B and 100C Electron Microscopes," Ultramicroscopy 5, 3-8.

24. Hayward S.B., D.A. Grano, R.M. Glaeser and K.A. Fisher (1978) "Molecular Orientation of Bacteriorhodopsin Within the Purple Membrane of Halobacterium halobium," Proc. Natl. Acad. Sci. 75, 4320-4324.

25. Hayward S.B. and R.M. Stroud (1981) "Projected Structure of Purple Membrane Determined to 3.7 Å Resolution by Low Temperature Electron Microscopy," J. Mol. Biol. 151, 491-517.

26. Henderson, R. and P.N.T. Unwin (1975) "Three-Dimensional Model of Purple Membrane Obtained by Electron Microscopy," Nature 257, 28-32.

27. Herrmann, K.H., D. Krahl and H.P. Rust (1978) "A TV System for Image Recording and Processing in Conventional Transmission Electron Microscopy," Ultramicroscopy 3, 227-235.

28. Howitt, D.G., R.M. Glaeser, and G. Thomas (1976) "The Energy Dependence of Electron Radiation Damage in l-Valine," J. Ultrastruc. Res. 55, 457-461.

29. Ichihara and Mizushima (1978) "Characterization of Major Outer membrane Proteins O-8 and O-9 of Escherichia coli K-12: Evidence that Structural Genes for the Two Proteins are Different," J. Biochem. (Tokyo) 83, 1095-1100.

30. Inokuchi, K., N. Mutoh, S. Matsuyama and S. Mizushima (1982) "Primary Structure of the ompF Gene that Codes for a Major Outer Membrane Protein of Escherichia coli K-12," Nucleic Acids Research 10, 6957-6968.

31. Inouye, M. (1979) "What is the Outer Membrane?," Bacterial Outer Membranes: Biogenesis and Functions, edited by M. Inouye (John Wiley and Sons Inc., New York) 1-12.

32. Inouye, M., J. Shaw and C. Shen (1972) "The Assembly of a Structural Lipoprotein in the Envelope of Escherichia coli," J. Biol. Chem. 247, 8154-8159.

33. Jaffe, J.S. and R.M. Glaeser (1982) "Preparation of Frozen Hydrated Purple Membrane For High Resolution Electron Microscopy," Proc. Electron Micro. Soc. Am. 40 72-73.

34. Jesior, J.C. (1982) "A New Approach for the Visualization of Molecular Arrangement in Biological Microcrystals," Ultramicroscopy 8, 379-384.

35. Joy, R.T. (1973) "The Electron Microscopical Observation of Aqueous Biological Specimens," Adv. Optical and E.M. 5, 297-352.

36. Kistler, J., U. Aebi and E. Kellenberger (1977) "Freeze-Drying and Shadowing a Two-Dimensional Periodic Specimen," J. Ultrastruc. Res. 59, 76-86.

37. Kuo, I.A.M. and R.M. Glaeser (1975) "Development of Methodology for Low Exposure, High Resolution Electron Microscopy of Biological Specimens," Ultramicroscopy 1, 53-66.

38. Lepault, J. and J. Dubochet (1980) "Preservation of Biological Specimens After Freezing," Proceedings of the European Congress on Electron Microscopy 2, 648-649.

39. Manning, P.A., A.P. Pugsley and P. Reeves (1977) "Defective Growth Functions in Mutants of Escherichia coli K12 Lacking a Major Outer Membrane Protein," J. Mol. Biol. 116, 285-300.

40. Manning, P.A. and M. Achtman (1979) "Cell-to-Cell Interactions in Conjugating Escherichia coli: the Involvement of the Cell Envelope," Bacterial Outer Membranes: Biogenesis and Functions, edited by M. Inouye (John Wiley and Sons Inc., New York) 409-447.

41. Matricardi, V.R., R.C. Moretz and D.F. Parsons (1972) "Electron Diffraction of Wet Proteins: Catalase," Science 177, 268-269.

42. Mizuno, T., M-Y. Chou and M. Inouye (1983) "A Comparative Study on the Genes for Three Porins of the Escherichia coli Outer Membrane: DNA Sequence of the

Osmoregulated ompC gene," J. Biol. Chem. 258, 6932-6940.

43. Nagata, F. and I. Ishikawa (1972) "Observation of Wet Biological Materials in a High Voltage Electron Microscope," Japanese J. Applied Physics 1239-1244.

44. Nakae, T. (1976) "Identification of the Outer Membrane Protein of E. coli That Produces Transmembrane Channels in Reconstituted Vesicle Membranes," Biochem. Biophys. Res. Commun. 71, 877-884.

45. Nakae, T. and H. Nikaido (1975) "Outer Membrane As a Diffusion Barrier in Salmonella typhimurium," J. Biol. Chem. 250, 7359-7365.

46. Nakamura, K., D.N. Ostrovsky, T. Miyazawa and S. Mizushima (1974) "Infrared Spectra of Outer and Cytoplasmic Membrane of Escherichia coli, Biochim. Biophys. Acta 332, 329-335.

47. Nakamura, K. and S. Mizushima (1976) "Effect of Heating in Dodecyl Sulfate on the Conformation and Electrophoretic Mobility of Isolated Major Outer Membrane Proteins from Escherichia coli K-12," J. Biochem. (Tokyo) 80, 1411-1422.

48. Nikaido, H., S.A. Song, L. Shaltiel and M. Nurminen (1977) "Outer Membrane of Salmonella XIV. Reduced Transmembrane Diffusion Rates in Pore-Deficient Mutants," Biochem. Biophys. Res. Commun. 76, 324-330.

49. Nikaido, H., E.Y. Rosenberg and J. Foulds (1983)

"Porin Channels in Escherichia coli: Studies with β-Lactams in Intact Cells," J. Bacteriol. 153, 232-240.

50. Nikaido, H. and E.Y. Rosenberg (1983) "Porin Channels in Escherichia coli: Studies with Liposomes Reconstituted from Purified Proteins," J. Bacteriol. 153, 241-252.

51. Overbeeke, N., H. Bergmans, F. van Mansfeld and B. Lugtenberg (1983) "Complete Nucleotide Sequence of phoE, the Structural Gene for the Phosphate Limitation Inducible Outer Membrane Pore Protein of Escherichia coli K-12," J. Mol. Biol. 163, 513-532.

52. Reimer, L. (1965) "Irradiation Changes in Organic and Inorganic Objects," Lab. Invest. 14, 1082-1096.

53. Richards, K.E. and R.C. Williams (1972) "Electron Microscopy of Aspartate Transcarbamylase and Its Catalytic Subunit," Biochemistry 11, 3393-3395.

54. Rosenbusch, J.P. (1974) "Characterization of the Major Envelope Protein from Escherichia coli, J. Biol. Chem. 249, 8019-8029.

55. Schindler, H. and J.P. Rosenbusch (1978) "Matrix Protein from Escherichia coli Outer Membrane Forms Voltage-Controlled Channels in Lipid Bilayers," Proc. Natl. Acad. Sci., 75, 3751-3755.

56. Sosinsky, G.E. (1983) "Structural and Physiological Studies on the Crystalline Membrane Particles in the Yeast Saccharomyces cerevisiae," Ph.D. Thesis.

57. Stenn, K. and G.F. Bahr (1970) "Specimen Damage Caused by the Beam of the Transmission Electron Microscope, A Correlative Reconsideration," J. Ultrastruc. Res. 31, 526-550.

58. Steven, A.C., B. ten Heggeler, R. Muller, J. Kistler and J.P. Rosenbusch (1977) "Ultrastructure of a Periodic Protein Layer in the Outer Membrane of Escherichia coli," J. Cell Biol. 72, 292-301.

59. Tanford, C., Y. Nozaki, J.A. Reynolds and S. Makino (1974) "Molecular Characterization of Proteins in Detergent Solutions," Biochemistry 13, 2369-2376.

60. Taylor, K.A. and R.M. Glaeser (1974) "Electron Diffraction of Frozen Hydrated Protein Crystals," Science 186, 1036-1037.

61. Taylor, K.A. and R.M. Glaeser (1975) "Modified Airlock Door For the Introduction of Frozen Specimens into the JEM 100B Electron Microscope," Rev. Sci. Instrum. 46, 985-986.

62. Taylor, K.A. and R.M. Glaeser (1976) "Electron Microscopy of Frozen Hydrated Biological Specimens," J. Ultrastruc. Res. 55, 448-456.

63. Tommassen, J. and B. Lugtenberg (1980) " Outer Membrane Protein e of Escherichia coli K-12 Is Co-Regulated with Alkaline Phosphatase," J. Bacteriol. 143, 151-157.

64. Unwin, P.N.T. and R. Henderson (1975) "Molecular

Structure Determination by Electron Microscopy of Unstained Crystalline Specimens," J. Mol. Biol. 94, 425-440.

65. Wallace, B.A. and R. Henderson (1981) "Location of the Carboxyl Terminus of Bacteriorhodopsin in Purple Membrane," Biophys. J. 39, 233-239.

66. Waldbillig, R.C., J.D. Robertson and T.J. McIntosh (1976) "Images of Divalent Cations in Unstained Symmetric and Asymmetric Lipid Bilayers," Biochim. Biophys. Acta 448, 1-14.

67. Williams, R.C. (1952) "Electron Microscopy of Sodium Deoxyribonucleate by use of a new Freeze-Drying Method," Biochim. Biophys. Acta 9, 237-239.

68. Williams, R.C. (1953) "A Method of Freeze-Drying for Electron Microscopy," Exptl. Cell Res. 4, 188-201.

69. Williams, R.C. (1981) "Morphology of Bovine Fibrinogen Monomers and Fibrin Oligomers," J. Mol. Biol. 150, 399-408.

70. Williams, R.C. and S. Fraser (1953) "Morphology of the Seven T-bacteriophages," J. Bacteriol. 66, 458.

71. Williams, R.C. and H.W. Fisher (1970) "Electron Microscopy of Tobacco Mosaic Virus under Conditions of Minimal Beam Exposure," J. Mol. Biol. 52, 121.

72. Williams, R.C. and H.W. Fisher (1970) "Electron Microscopy with Minimal Beam Damage," Proc. Electron Micro. Soc. Am. 28, 304-305.

73. Wyckoff, R.W.G. (1946) "Frozen-Dried Preparation for the Electron Microscope," Science 104, 36-37.

74. Yamada, H. and S. Mizushima (1978) "Reconstitution of an Ordered Structure from Major Outer Membrane Constituents and Lipoprotein-Bearing Peptidoglycan Sacculus of Escherichia coli," J. Bacteriol. 135, 1024-1031.

75. Yamada, H. and S. Mizushima (1980) "Interaction Between Major Outer Membrane Protein (O-8) and Lipopolysaccharide in Escherichia coli K-12," Eur. J. Biochem. 103, 209-218.

76. Zalman, L.S.,H. Nikaido and Y. Kagawa (1980) "Mitochondrial Outer Membrane Contains a Protein Producing Nonspecific Diffusion Channels" J. Biol. Chem. 255, 1771-1774.

TECHNICAL INFORMATION DEPARTMENT
LAWRENCE BERKELEY LABORATORY
UNIVERSITY OF CALIFORNIA
BERKELEY, CALIFORNIA 94720